Journal of Structural Geology 134 (2020) 103994

Contents lists available at ScienceDirect

Journal of Structural Geology

journal homepage: http://www.elsevier.com/locate/jsg

Eocene seismogenic reactivation of a Jurassic ductile shear zone at Cap de Creus, Pyrenees, NE Spain

Reinoud L.M. Vissers [a,*], Morgan Ganerød [b], Gill M. Pennock [a], Douwe J.J. van Hinsbergen [a]

[a] Department of Earth Sciences, University of Utrecht, Budapestlaan 4, 3584 CD, Utrecht, the Netherlands
[b] Geological Survey of Norway, Solid Earth Geology, Leiv Eirikssons vei 39, 7491, Trondheim, Norway

ARTICLE INFO

Keywords:
Cap de Creus
Pyrenees
Pseudotachylyte
Fault reactivation
$^{40}Ar/^{39}Ar$ dating

ABSTRACT

The Cap de Creus peninsula in NE Spain exposes Variscan amphibolite-facies rocks, transected by greenschist-facies mylonitic shear zones accommodating displacements of up to 1 km. One of these shear zones contains pseudotachylytes with 1–4 mm thick fault veins and cm-scale high-angle injection veins and breccias. The pseudotachylyte matrix encloses mm-to μm-scale wallrock fragments and consists of ultrafine biotite and feldspar, often with a microporphyritic structure suggesting crystallization from a melt. Recent dating of the host shear zone yielded a Jurassic (170-160 Ma) age. Here we present $^{40}Ar/^{39}Ar$ dating of the pseudotachylytes yielding Early Eocene ages between 52.76 ± 1.64 Ma and 44.55 ± 0.77 Ma, indicating Alpine brittle faulting at times that Jurassic low-angle ductile shears had been tilted to their present vertical position following Alpine thrusting in the Pyrenees. The kinematics of the pseudotachylytes suggest strike-slip reactivation along the host shear zone, consistent with plate-kinematic analyses indicating coeval Iberia - Europe motion dominated by strike-slip. The dimensions of the pseudotachylyte-bearing zone and estimated brittle displacements suggest a moment magnitude of ~4.7–4.9. The average thicknesses of the fault veins indicate deformation at ≥4 km depth, an energy density of ~9.10^6 J/m^2 and a frictional resistance of ~23 MPa.

1. Introduction

Fault-related pseudotachylytes are generally considered to result from frictional heating during coseismic brittle faulting (Sibson, 1977; Grocott, 1981; Swanson, 1992; Magloughlin, 1992; Kirkpatrick et al., 2009; Toy et al., 2011). Field studies have documented such tectonic pseudotachylytes from dominantly cataclastic rocks as well as from ductile mylonitic environments. Conceptual models for deep crustal-scale fault zones, in particular strike-slip faults (Sibson, 1983; Swanson, 1992), suggest that fault-related pseudotachylytes may be expected to develop from deep greenschist facies levels around 12–16 km depth to entirely brittle levels around 2–4 km (Sibson and Toy, 2006). Pseudotachylytes that developed at deep levels may thus overprint foliated structures formed during slow ductile creep. Pseudotachylytes from such regimes have been reported, e.g., from the Outer Hebrides Thrust of northwest Scotland (Sibson, 1977, 1980), the Musgrave block in central Australia (Wenk and Weiss, 1982), from mylonitic gneisses of the Barthélémy Massif in the French Pyrenees (Passchier, 1982, 1984), the Late Paleozoic mylonites of the southern coast of Maine (Swanson, 1988), and from the Møre-Trøndelag Fault Zone in W Norway (Sherlock et al., 2004). The presence of fault-related pseudotachylytes in these sheared rocks may reflect the progressive interplay of mainly ductile and genuinely brittle processes during the waning stages of ductile shear, possibly associated with a long-term gradual transition to the brittle field. Alternatively, these structures may have developed completely unrelated to the earlier shear history, during an essentially much later, brittle reactivation event.

This paper is concerned with pseudotachylyte structures in a greenschist facies shear zone at Cap de Creus (E Pyrenees, Spain). The region is world-famous among structural geologists for the excellent exposure of ductile shear zones (e.g., Carreras et al., 1977, 1980; Druguet, 1997; Carreras, 2001, and references therein; Fusseis et al., 2006; Fusseis and Handy, 2008). Despite detailed structural research in the area, however, the pseudotachylytes of Cap de Creus have so far, to the best of our knowledge, not been described in the structural literature. In this paper, we aim (1) to document pseudotachylyte structures and microstructures from a shear zone in the Cap de Creus area, (2) to present the results of $^{40}Ar/^{39}Ar$ dating of the pseudotachylytes to assess the temporal and tectonic context within which they formed, and (3) to estimate seismic source parameters associated with the development of

* Corresponding author.
E-mail address: r.l.m.vissers@uu.nl (R.L.M. Vissers).

https://doi.org/10.1016/j.jsg.2020.103994
Received 18 September 2019; Received in revised form 16 January 2020; Accepted 17 January 2020
Available online 7 February 2020

the pseudotachylytes. This allows us to place the structures, dating results and inferred seismic parameters in the larger scale context of the Alpine orogeny as outlined in the discussion below.

2. Geological setting of the pseudotachylyte-bearing shear zone

Cap de Creus in NE Spain forms the easternmost end of the Pyrenees, the Alpine fold-thrust belt that formed by collision of Iberia and Eurasia. The Pyrenees contain a core known as the Axial Zone exposing Paleozoic rocks that were intensely deformed and metamorphosed during the Variscan orogeny (Zwart, 1979), and a Mesozoic-Cenozoic cover of mostly non-metamorphic sediments that are only affected by Alpine deformation processes (Fig. 1, inset). The region around Cap de Creus belongs to the Axial Zone and exposes uppermost Proterozoic to Cambrian, dominantly siliciclastic sediments (Carreras, 2001; Castiñeiras et al., 2008), metamorphosed during the Variscan orogeny to LP-HT amphibolite facies metagreywackes and cordierite-sillimanite biotite schists up to migmatite-grade (e.g., Druguet, 1997; see Fig. 1). The area is thus dominated by dark-coloured metagreywackes and metapelites, with an intensely developed foliation parallel to the axial planes of isoclinal folds, often refolded by second-generation tight folds with crenulated structures along their axial planes. These structures, conveniently described in terms of first and second generation (D1, S1 and D2, S2) deformations, show N–S to NE-SW oriented trends and are both associated with Variscan LP-HT metamorphism. In addition, coarse-grained pegmatitic granitoids (Fig. 1) have intruded the higher-grade rocks mainly between the first and second deformation (Druguet et al., 1997). Granitoids and migmatites at Cap de Creus are not dated, but nearby exposures of these rocks further west yielded ages of 299–290 Ma (Druguet et al., 2014).

A set of commonly SE-NW and less frequently EW striking, greenschist facies ductile shear zones transect the amphibolite facies Variscan structure. They are developed in the Cap de Creus area at a regional scale (Carreras, 2001; Fusseis et al., 2006) and show estimated displacements of the order of 1 km. One of these shear zones, consisting of an intricately anastomosing network of smaller scale shears, separates the rocks around the Cap de Creus light house from the westerly part of the area (Fig. 1). This shear zone, running from cala Cullaró in the north via cala Culip to cala Jugadora and cala Fredosa to the S and SE, has a moderate to steep dip to the NE. Both the exposures near cala Cullaró and the branch running from cala Culip to cala Fredosa (Fig. 1) contain pseudotachylytes, developed along an intensely sheared mylonitic matrix as

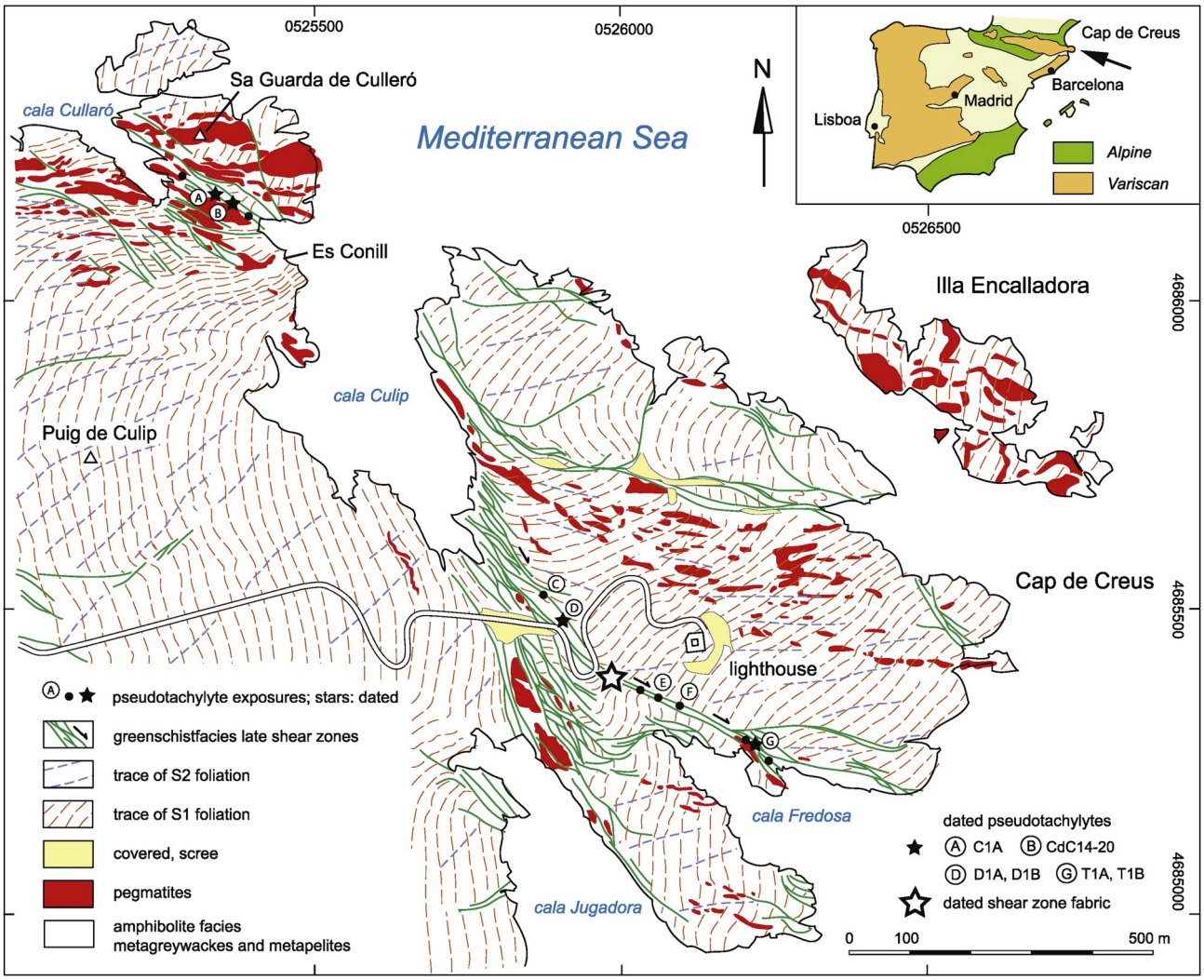

Fig. 1. Structural form surface map of the easternmost Cap de Creus peninsula, slightly modified after Druguet et al. (1997). Location in NE Spain shown on inset map (arrow). The Variscan tectonic fabrics (S1 and S2) are transected and deflected by mostly SE-NW and fewer E-W striking greenschist facies shear zones. White star denotes location of shear zone sample CdC-13, used for Ar–Ar dating of the shear fabric (Vissers et al., 2017). Large black star in the NW indicates location of dated pseudotachylyte vein at locality B. Studied exposures of pseudotachylyte in the main shear zone between cala Culip and cala Fredosa are shown as black dots and, occasionally, as small stars indicating pseudotachylytes used for additional dating.

described below.

The Cap de Creus shear zones formed under retrogressive metamorphic conditions and their age has for a long time been the subject of debate, since both Alpine and Variscan ages have been proposed (see, e.g., Carreras, 2001). Recent muscovite $^{40}Ar/^{39}Ar$ dating of shear zones in the area (Vissers et al., 2017) have yielded Jurassic (Oxfordian) ages between 159.33 ± 0.43 and 175.18 ± 1.10 Ma (all dates are quoted at the 95% confidence level). The dating of muscovite from the pseudotachylite-hosting cala Culleró – cala Fredosa shear zone gave a 162.45 ± 0.96 Ma $^{40}Ar/^{39}Ar$ age (the location of the dated exposure is indicated in Fig. 1 by a white star). One shear zone in the region, in addition, yielded an age of 58.57 ± 0.55 Ma (Vissers et al., 2017).

Vissers et al. (2017) showed that the present steep dip of the shear zones and the more or less horizontal strongly attenuated metamorphic field gradient are most likely the result of Alpine tilting and represent a Jurassic low-angle extensional shear zone that formed at the eastern Iberian margin. Extensive offshore geophysical imaging on the eastern Iberian margin has demonstrated that during the middle Jurassic eastern Iberia underwent hyperextension (Etheve et al., 2018) during slow opening of the Alpine Tethys ocean (Vissers et al., 2013), in which context the low-angle extensional shear zones of Cap de Creus fit well (Vissers et al., 2017; van Hinsbergen et al., 2019).

3. Structures of the cala Cullaró – cala Fedrosa shear zone

3.1. Ductile shear structures and associated assemblages

The shear zone is characterized by intense stretching and drag of earlier S1 and S2 foliations in the metapsammitic and pelitic wall rock, and an intensely developed mylonitic foliation Sm dominating the central parts of the shear zone (Fig. 2a and b). In many localities, asymmetric extensional crenulation cleavages (e.g. Platt and Vissers, 1981) consistently indicate top-to-the-SE motion (Fig. 2c), and trains of small-scale isoclinal folds with axial planes inclined to the mylonitic foliation equally suggest movement of the hanging wall to the SE, i.e., a dextral sense of motion in map view (Fig. 1). The mylonitic shear zone rocks are notably lighter coloured than the adjacent biotite-rich wall rock due to greenschist facies alteration of the precursor amphibolite facies assemblage (e.g., Fusseis and Handy, 2008). The greenschist facies mylonites are commonly fine-grained (grainsizes of 100 ?m or less) and are dominated by oriented muscovite and biotite occasionally interleaved with chlorite, quartz, and often albite (Fig. 2d), whilst several samples also contain clinozoisite. Some of the mylonitic schists are very rich in mica (≫ 50%). In such mica-rich rocks, extensional crenulation cleavage planes may be well developed (Fig. 2d) and decorated with very fine-grained intergrowths of chlorite and biotite (Fusseis and Handy, 2008). Porphyroclasts of colourless mica and feldspar, as well as occasional mica-feldspar pseudomorphs after andalusite, may occur enclosed in the fine-grained mylonitic matrix.

3.2. Pseudotachylyte structures and microstructures

At several localities in the shear zone pseudotachylytes are exposed (black dots and stars in Fig. 1). The geometry of these structures suggests that they are relatively late features. Concordant veins of dark very-fine-grained to cryptocrystalline material, either of variable thickness or almost perfectly planar, may occur at different levels in the shear zone (Fig. 3a). Their common persistence over several meters and their very sharp contacts with the mylonitic wall rock strongly suggest that these veins are fault veins (Sibson, 1977). The veins may show clear variations in thickness reminiscent of pinch-and-swell structures with a wavelength of one to a few dm, but where they are approximately planar they commonly show thicknesses between 1 and 4 mm, with a mean of 2 mm. They may also be discordant to the main mylonitic foliation, truncating and cutting across marker horizons (Fig. 3b). Associated with the fault veins are usually small, high-angle tapering veins interpreted as

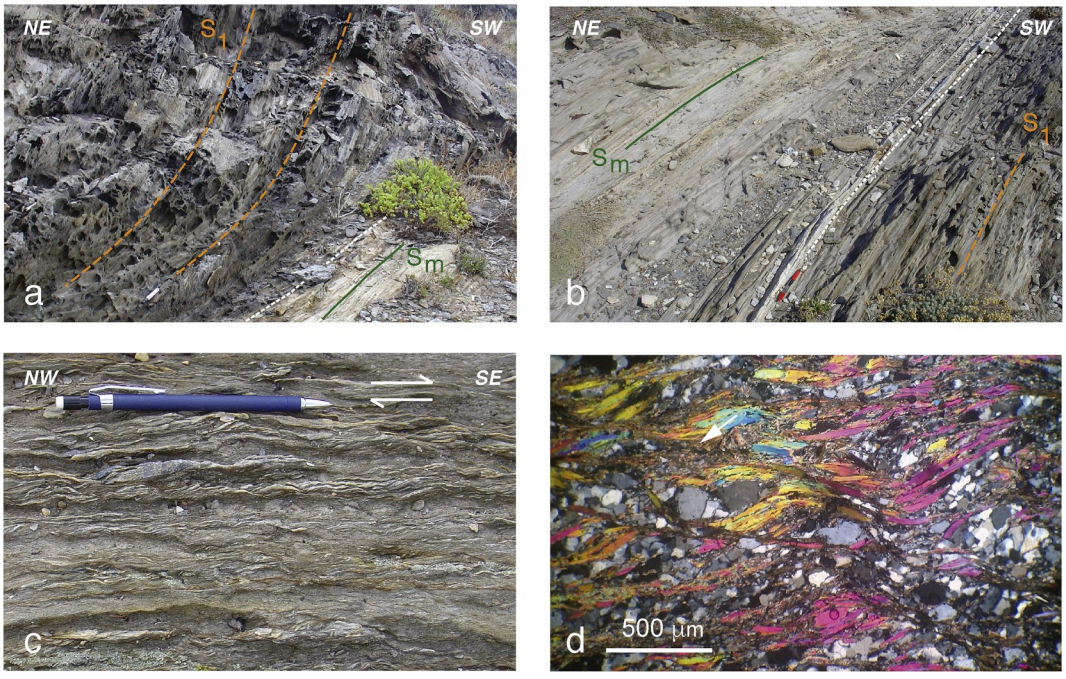

Fig. 2. Ductile shear structures of the pseudotachylyte-bearing shear zone between cala Culip and cala Fredosa. (a) Gradual change in orientation of the main S1 foliation in the dark biotite-sillimanite wall rock into the plane of the shear zone (Sm). Note light colour of shear zone rocks almost devoid of biotite, transition accentuated by dashed white line. (b) Similar structure, wherein S1 is deflected into Sm, along the footwall of the shear zone, again with a gradual decrease in biotite content (across dashed white line) towards the light coloured mylonitic shear zone rocks. (c) Wavy aspect of mylonitic foliation due to ubiquitous asymmetric extensional crenulations consistently indicating dextral (top-to-the-SE) motion. (d) Shear zone microstructure dominated by asymmetric extensional crenulation cleavage decorated with very fine-grained intergrowths of chlorite and biotite (arrow). This sample was used for Ar–Ar dating of the shear zone fabric (see Fig. 1, white star). (For interpretation of the references to colour in this figure legend, the reader is referred to the Web version of this article.)

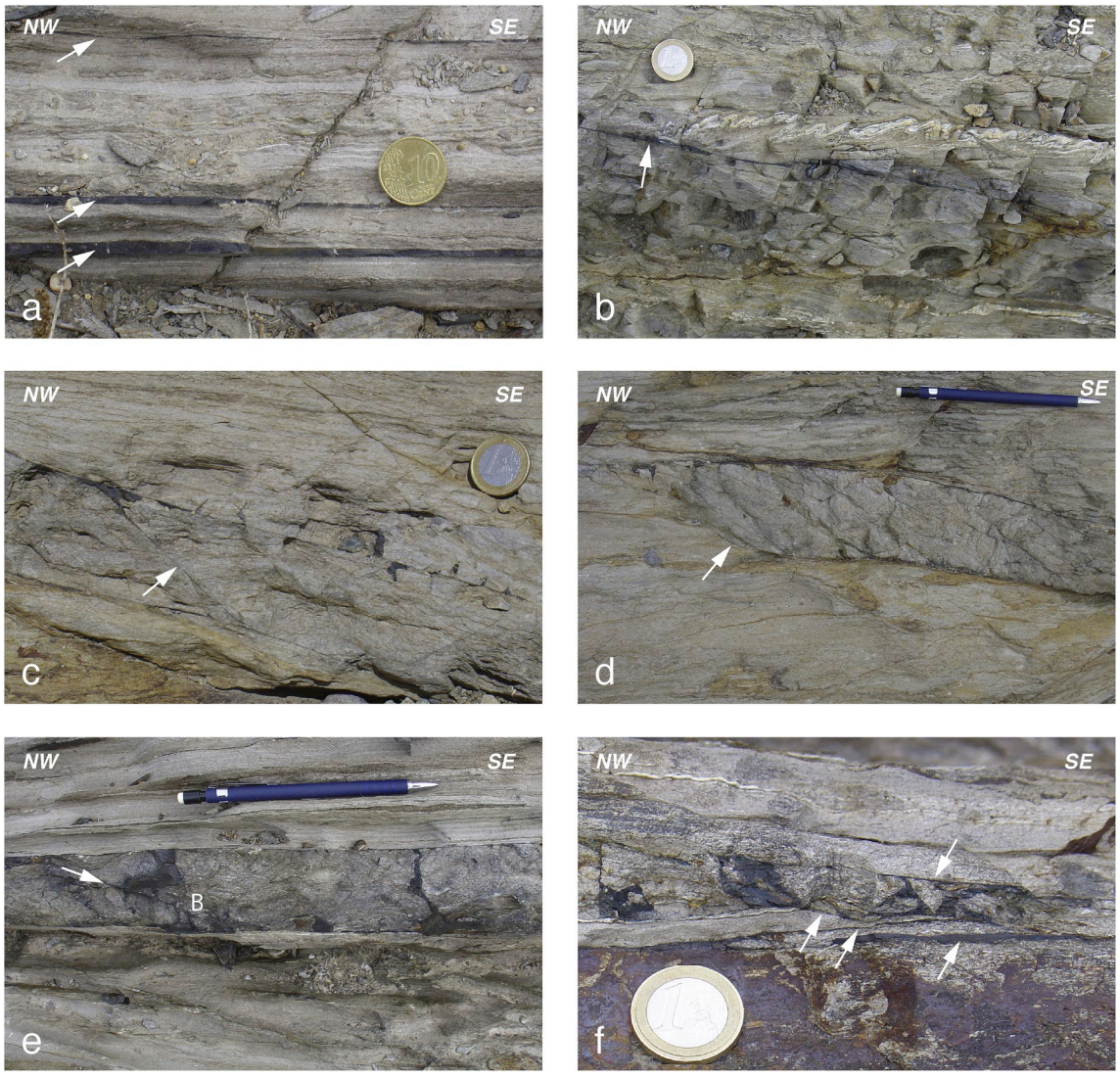

Fig. 3. Pseudotachylyte structures in the cala Culip – cala Fedrosa shear zone; locations of exposures shown in Fig. 1 (a) Concordant planar fault veins (arrows) parallel to main mylonitic foliation in exposure D. (b) Discordant fault vein in exposure E showing pinch-and-swell geometry (arrow), and cutting at low angle across mylonitic foliation accentuated by foliation-parallel train of inclined folds. (c) Slightly discordant pseudotachylyte-bearing fault vein in exposure F showing small tapering injection veins, and occasional east-dipping pseudotachylyte bearing fractures (arrow). (d) Ladder pattern of partly pseudotachylyte-bearing fractures in between two subparallel fault veins, exposure F. Arrow points to termination of lower fault vein curving upward. (e) Network of injection veins in between two fault veins, grading to pseudotachylyte breccia (B), exposure D. Note right-dipping veinlet with Riedel fracture orientation (arrow). (f) Breccia with glassy pseudotachylyte matrix in exposure G. Arrows indicate generation surfaces.

injection veins (Toy et al., 2011, Figs. 3c and 4a). The fault vein – injection vein geometries such as observed at Cap de Creus are considered to be a principal characteristic feature of tectonic pseudotachylytes (Sibson and Toy, 2006).

More complex observed pseudotachylyte geometries range from ladder structures (Sibson, 1977) (Fig. 3d) to breccias (Fig. 3e and f). These structures, equivalent to the pseudotachylyte generation zones of Grocott (1981), are essentially formed by two subparallel fault veins linked by high-angle injection vein structures, where larger amounts of dark pseudotachylyte separate increasingly isolated fragments of wall rock. Small-scale Riedel-type fractures decorated by pseudotachylyte (Fig. 3e) occasionally contribute to the brecciation. The dilatation necessarily involved in the development of these structures confirms that they are genuinely brittle.

At this stage, it needs to be emphasized that the field observations as such do not prove that the glassy cryptocrystalline material in the fault and injection veins illustrated in Fig. 3 result from frictional heating during coseismic motion along the pertinent fault surfaces. We therefore proceed to inspect the microstucture of the pseudotachylyte in search for features diagnostic for the former presence of a melt phase. Fig. 4a shows a fault vein sampled from exposure A near the northwestern end of the cala Culleró - cala Fedrosa shear zone. Numerous fine-grained clasts in the margin of the fault vein show a marked shape preferred orientation (Fig. 4b) that could have developed as the clasts were transported by flow of a matrix melt, whilst a millimetre-scale isoclinal fold in the centre of the fault vein (Fig. 4a) seems consistent with flow of an essentially fluid (liquid) phase (Fig. 4a, note fold hinge F). In addition, some small fragments enclosed in the dark pseudotachylyte matrix show embayments compatible with corrosion by a melt (Fig. 4b and c). The micron-scale pseudotachylyte microstructure, illustrated in the backscattered electron micrographs of Fig. 4c and d, is characterized by 20 ?m scale clasts embedded in a matrix of 1–5 ?m size platelets of biotite intergrown with Ca-poor plagioclase and occasional quartz with an ultrafine grained microporphyritic texture that is clearly igneous (Fig. 4e and f). Semi-quantitative microchemical analyses of the ultrafine grained material are presented in the supplementary data. A general

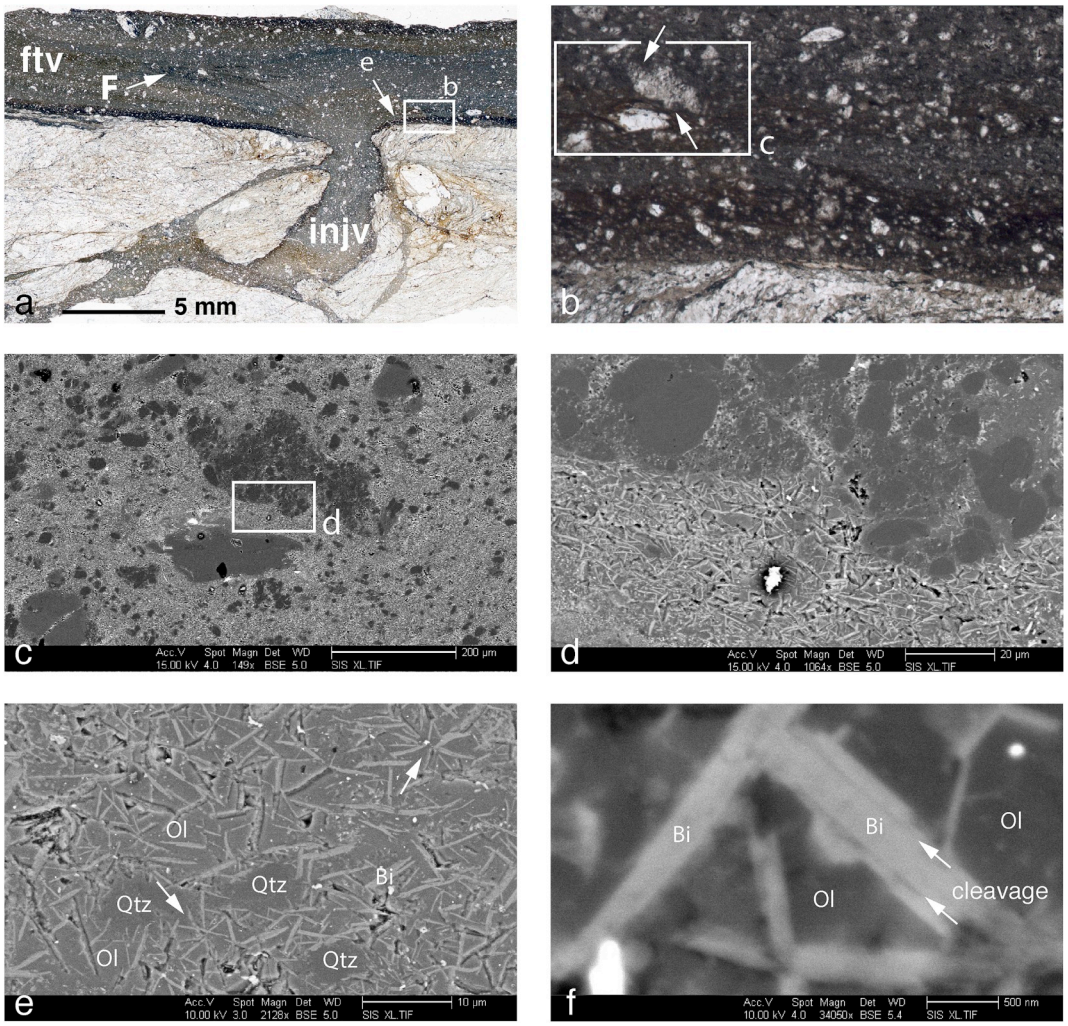

Fig. 4. Microstructure of pseudotachylyte from exposure A near cala Cullaró. (a) Light micrograph (plane polarized light) of fault vein (ftv) with injection vein (injv). Note zoned structure of the vein resulting from isoclinal fold (F). (b) Detail of a, showing dark pseudotachylyte matrix with numerous tiny clasts. Clast in upper left corner shows embayments (arrows) suggesting corrosion by a melt. Note preferred orientation of tiny clasts in the lower margin of the vein, which is less prominent away from the vein margin. (c) Backscattered electron micrograph of detail outlined in b. The pseudotachylyte is made up of numerous 10–20 ?m scale clasts of mostly quartz and few larger rock fragments with clear embayments in an ultrafine and porous crystalline matrix. (d) Detail of c showing crystallite microstructure made up of 1–10 ?m size platelets of biotite intergrown with Ca-bearing plagioclase (oligoclase) and occasional quartz, adjacent to and partly corroding rock-fragment. (e) Backscattered electron micrograph showing clearly igneous microstructure of ultrafine grained pseudotachylyte matrix, made up of euhedral biotite grains (Bi) and intergrown anhedral oligoclase (Ol), and occasional grains of quartz (Qtz). Arrows point to radially arranged biotite grains. (f) Detail of oligoclase-biotite microstructure showing biotite grain with typical mica cleavage (arrows).

lack of typical devitrification microstructures like spherulites, reported from pseudotachylytes by other workers (see e.g., Spry, 1969), lead us to interpret the biotite-feldspar matrix as the product of crystallization from a melt rather than devitrification of a glass phase, but we note that occasional aggregates of radially arranged biotites (Fig. 4e) may well have grown from initially dendritic nuclei.

3.3. Kinematics of the pseudotachylytes

Kinematic interpretations of the ductile shear zone structures at Cap de Creus are generally straightforward because of the excellent exposure of kinematic indicators (e.g., Carreras, 2001). The kinematics of the pseudotachylyte bearing fault veins, however, is more problematic because the shear direction data are largely limited to few faint, groove-like lineations on fault vein – wall rock interfaces. The significance of these faint lineations on the pseudotachylyte fault veins is enigmatic, but we hypothesize that they originate from a cataclastic precursor at the onset of frictional melting, because the melt clearly has a proportion of rigid clasts.

An interesting exposure to study kinematic aspects of the pseudotachylytes was found in locality G (Fig. 1) illustrated in Fig. 5. The exposure allows a view onto the plane of a concordant fault vein parallel to the mylonitic foliation Sm (Fig. 5a). The fault vein is partly eroded, revealing numerous small injection veins in the wall rock immediately underneath. A detail is shown in Fig. 5b, in which at least two veins show an en-echelon tension gash geometry suggesting that the two veins are in fact shear structures in the plane of Sm. As the orientation of the erosion surface approximates that of the mylonitic foliation Sm, hence of the concordant fault vein, we may analyse the distribution of the various injection veinlets in the plane of the fault vein. The result is shown in Fig. 5c and d. The rose diagram shows a distribution that at least qualitatively matches the expected distribution of faults in the XY plane when oriented as in Fig. 5e. The data suggest a shallowly SE plunging principal displacement axis x, close to the trend of a set of joints (j) in the black pseudotachylyte material that might represent tensile structures perpendicular to the principal direction of shortening in the plane of Sm. These results are consistent with a subhorizontal direction of motion parallel to the faint groove-like lineations on fault vein walls (see also

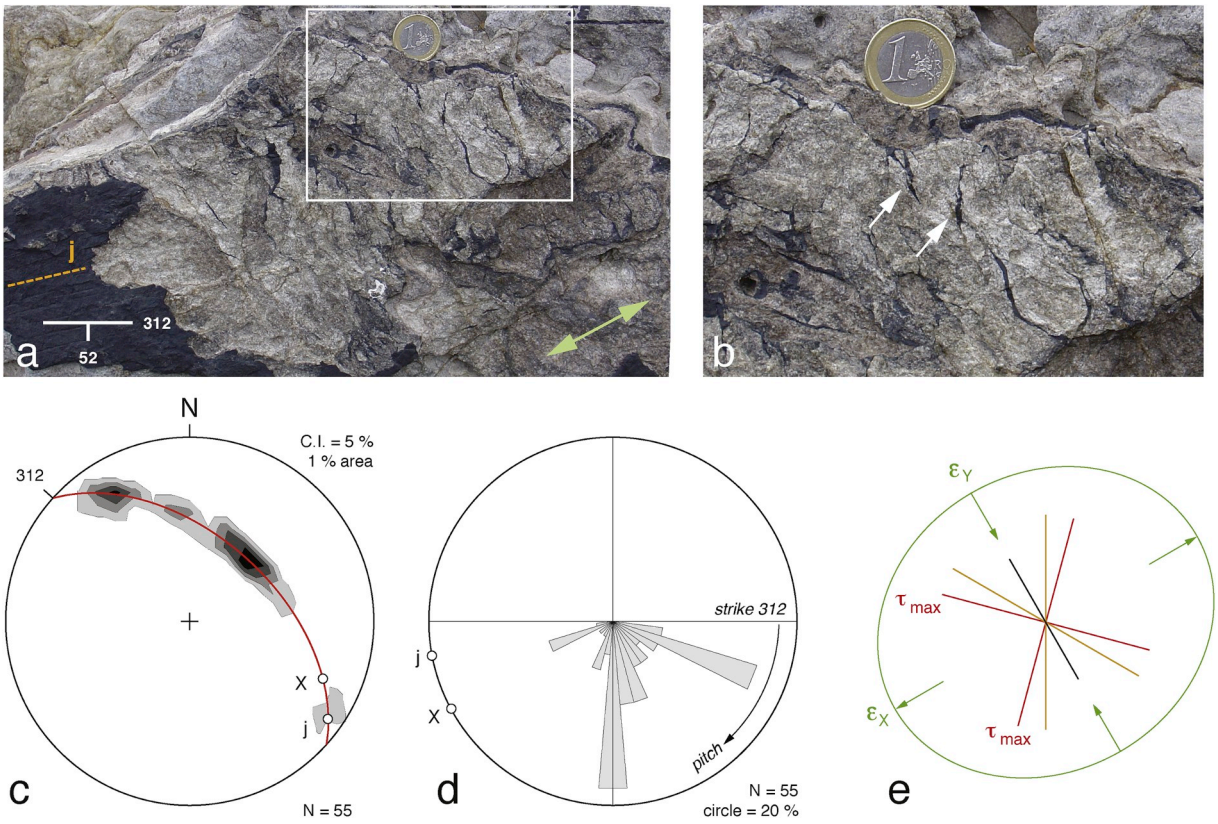

Fig. 5. (a) Exposure of concordant pseudotachylyte vein and associated small injection veins at location G, viewed perpendicular to the main foliation. The dark pseudotachylyte in the lower left is partly eroded such that the geometry and trends of the injection veinlets can be studied. Note set of joints (j) developed in the pseudotachylyte layer and accentuated by dashed orange line. (b) Detail showing injection veins made up of minute en-echelon gashes. (arrows). (c) Equal area, lower hemisphere projection showing contoured trends of 55 veinlet-foliation intersections. Main foliation Sm and concordant fault vein indicated by red great circle. X represents approximate brittle stretching direction inferred from orientations of the injection veins, j the trend of the joints in the pseudotachylyte vein. (d) Rose diagram showing distribution of pitches of the veinlet-foliation intersections, i.e. referred to the strike of the generation surface. (e) Qualitative distribution of brittle structures referred to principle displacement axes (ε_X and ε_Y) in the plane of the foliation, with shear fractures in orange and tension fractures in black. Comparison with the rose diagram suggests a shallowly SE plunging largest displacement axis ε_X. (For interpretation of the references to colour in this figure legend, the reader is referred to the Web version of this article.)

Fig. 11 below).

Whilst the above analysis suggests a subhorizontal direction of motion along the pseudotachylyte fault veins, the associated movement sense remains unclear. With the aim to elucidate the movement sense, we address a pseudotachylyte exposure (locality D in Fig. 1) comprising an >6 m long section with multiple fault vein structures (Fig. 6). In the NW part of the exposure the structure is dominated by a system of two roughly concordant fault veins with pseudotachylyte-bearing breccia in between (Fig. 3e), passing to the SE into a single fault vein with several pseudotachylyte lenses and high-angle injection veins. At less than 0.5 m below this fault vein, two discordant fault veins cut downward to the SE, and enclose a dm-scale duplex structure of at least four slices, each bounded by pseudotachylyte-bearing faults (Fig. 6b and c). The orientation of the outcrop is favourable for kinematic interpretation of the ductile structure, because the mylonitic foliation is roughly perpendicular to the erosion surface, with the ductile stretching direction approximately in the plane of the outcrop. Likewise, the fault vein structures are roughly perpendicular to the erosion surface and the faint lineations that may reflect the direction of brittle motion are again oriented in the plane of the outcrop. This implies that the duplex structure of Fig. 6 can potentially be restored. Fig. 7 shows a restoration of the structure assuming that the duplex geometry was formed in four single jerks (illustrated in Fig. 7b–e), and that fault veins may have slightly been curved as a result of slow post-seismic deformation. Three out of four of the associated displacements are NW-directed and resemble thrusts, whilst motion along fault 2 is SE directed. Note that the fault structures tend to shorten, hence thicken the mylonite zone. As the restoration does not really pose geometrical problems, it is hypothesized that the restoration may be valid and that the duplex structure indeed reflects the cumulative effect of at least four pseudotachylyte-generating fault motions, with estimated displacements of about 15, 5–10 and 25–40 cm respectively, while the displacement during the last stage (fault 4 in Fig. 7d and e) is not well constrained. It is unknown if the four stages of motion are sequential within one phase of brittle deformation, or that they represent different phases. As opposed to the top-to-the-SE ductile shear sense of the host mylonites, the thrust-like motions along the duplex forming faults indicate top-to-the-NW motion, i.e., a sinistral movement sense in map view, except for a small top-to-the-SE displacement of 5–10 cm along the stage 2 fault, consistent with the orientation of the Riedel fracture shown in Fig. 3e. For the overlying concordant fault veins higher in the exposure there are no constraints on the associated displacements.

At this stage, we emphasize that the pseudotachylyte structures documented here at Cap de Creus are clearly younger than the ductile shear zone structures. Irrespective of the excellent degree of exposure, we have not found any pseudotachylyte with evidence of subsequent ductile shearing, expected in case the pseudotachylytes and the shear structures were broadly coeval (such as e.g. described by Sibson (1977) from the Outer Hebrides). The opposed kinematics of the pseudotachylytes relative to that of the ductile shearing in the host rock and the overprinting relationships both suggest that the brittle deformation was not coeval with the ductile shear. Instead, the field data suggest that the

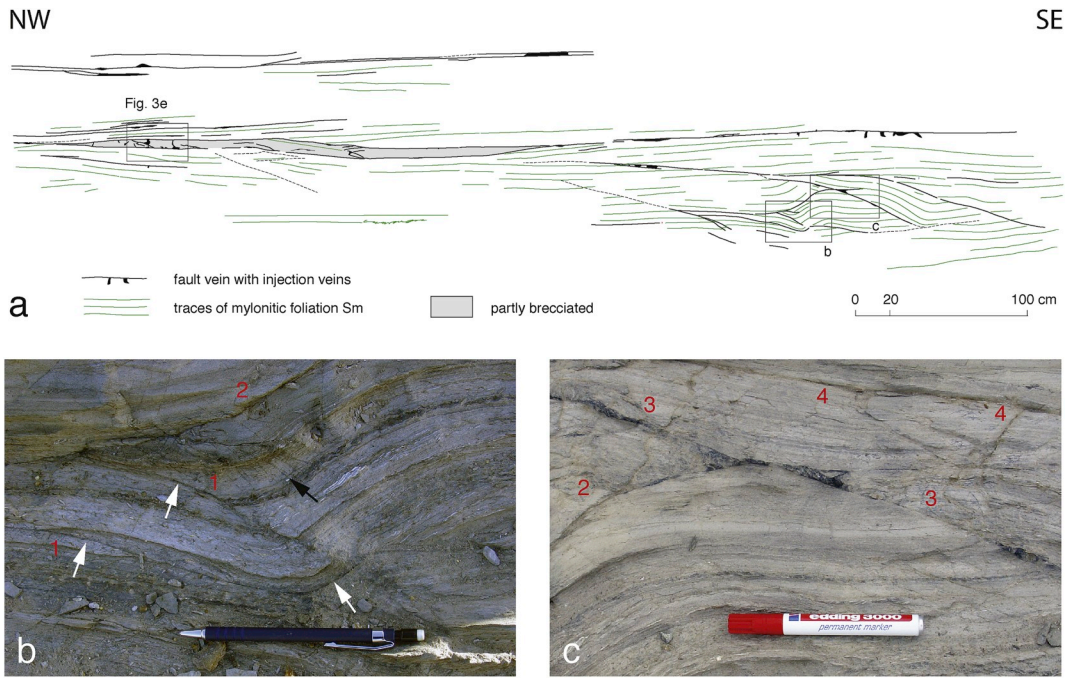

Fig. 6. (a) Pseudotachylyte geometry in exposure D, showing dominantly concordant fault veins but also discordant veins mostly cutting down to the SE. Main mylonitic foliation in green has an average dip of 55° to the NE, ductile stretching lineations plunge shallowly to the NW, whilst the erosion surface of the exposure dips towards the observer. This allows a view of the structure roughly parallel to the foliation, with the ductile motion in the plane of the outcrop. Note complicated duplex structure defined by pseudotachylyte-bearing faults at the SE side of the outcrop, analyzed in Fig. 7 (b) Detail of the early fault structure. Note that veins of the first (white arrows) and second stages were presumably affected by open folding before being cut by the younger faults 3 and 4 shown in (c). Note faint cleavage developed in the core of the synform (black arrow) suggesting a stage of ductile deformation by pressure solution. (c) Interaction of third stage fault vein with second stage vein. For further explanation see text. (For interpretation of the references to colour in this figure legend, the reader is referred to the Web version of this article.)

pseudotachylytes reflect a younger, brittle seismogenic overprint post-dating ductile shearing.

4. $^{40}Ar/^{39}Ar$ dating of the pseudotachylytes

Our field study of the cala Culleró – cala Fredosa ductile shear zone reveals ubiquitous evidence of a brittle overprint by pseudotachylyte-type fracture geometries. The associated fault veins are, in most cases, approximately concordant with the earlier mylonitic shear zone foliation, whilst less frequent discordant fault veins and injection veins clearly cut the ductile structures. As emphasized above, these geometrical relationships can be interpreted in two ways: (1) the pseudotachylyte structures may have developed progressively during the waning stages of ductile shear which, given the Jurassic age of the shear zone, would imply a Jurassic age of the pseudotachylytes, or (2) these structures developed completely unrelated to the earlier shear history during an essentially much later brittle deformation event. To distinguish between these different options, we have employed the stepwise heating $^{40}Ar/^{39}Ar$ technique to unravel the timing of pseudotachylyte formation. Obtaining age constraints of fault-generated pseudotachylytes can be an analytical challenge since they are most exclusively heterogeneous and can contain a complex mixture of minerals contained in the melt matrix with different diffusive properties and varying degrees of entrained unmelted host rock clasts (Di Vincenzo et al., 2004) which may disturb and/or elevate the apparent ages away from their formation ages. Despite of these challenges, several attempts have succeeded in obtaining reliable geochronology by careful data interpretation using stepwise heating and/or high resolution UV laser extraction methods, usually in tandem with microstructural analysis at different scales (e.g. Wenk et al., 2000; Di Vincenzo et al., 2004; Sherlock et al., 2004; Pennacchioni et al., 2006; Sherlock et al., 2009; Zanchetta et al., 2011; Di Vincenzo et al., 2013; Di Vincenzo et al., 2019).

We have selected pseudotachylyte samples from four different exposures along the shear zone (Fig. 1, exposures A, B, D and G; stars denote samples C1A at A, CdC14-20 at B, D1A and D1B at D, and T1A and T1B at G, see also Fig. 9 below). In view of a possible heterogeneity of the pseudotachylyte ages, we choose to test the reproducibility of the results by analyzing several splits of samples C1A, D1A and D1B. In addition to cm-scale sample CdC14-20 from exposure B, we prepared polished slabs and thin sections of pseudotachylite fault and injection veins from the other exposures (A, D and G), and used a microsaw to select small pieces (~2–3 mm) for age dating to allow control on the microstructure of the dated samples.

4.1. Method and $^{40}Ar/^{39}Ar$ analytical protocol

The sample of the pseudotachylyte from locality B was hand-crushed using an agate pestle and mortar, and one piece (~0.3 mm) was separated from the crushed material. The sample was packed in an aluminum capsule together with the Taylor Creek Rhyolite (TCR) flux monitor standard along with pure (zero age) K_2SO_4 and CaF_2 salts. Small fragments from the other three exposures (A, D and G) were prepared similarly. The samples were irradiated at IFE (Institutt for Energiteknikk, Kjeller, Norway) in two irradiations. The raw data and the correction factors for the production of isotopes from Ca and K can be found in the supplementary dataset X.X The samples were placed in a 3.5 mm pit size aluminum sample disk and step heated using a defocused 3.5 mm laser beam with a flat energy spectrum (Photon Machines Fusions 10.6). The extracted gases from the sample cell were first exposed to a piston free Striling cryochiller held at −130 ?C to trap potential water vapor, then further expanded into a two-stage low volume extraction line (c. 300 cm^3), both stages equipped with SAES GP-50 (st101 alloy) getters, the first running hot (c. 350 °C) and the second held at room temperature. Argon isotope compositions were analyzed

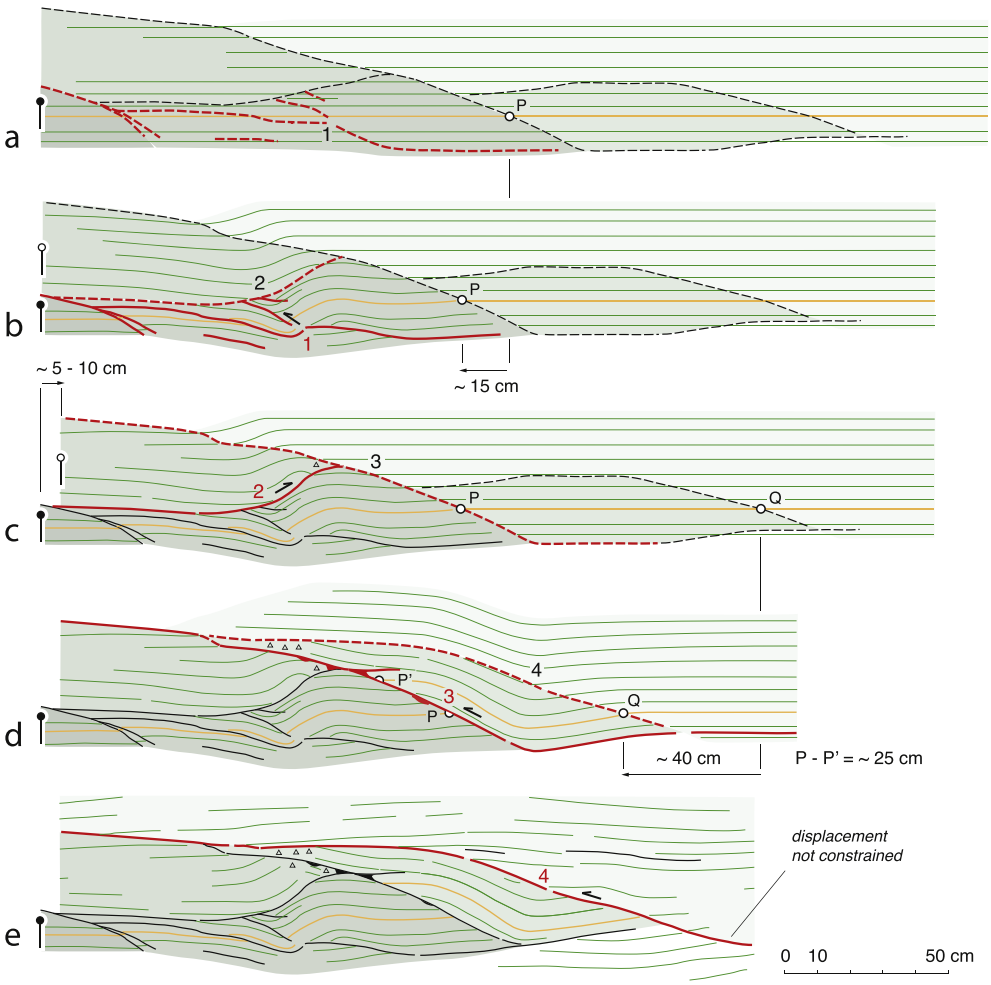

Fig. 7. (a) Restored section across the duplex structure at the SE side of exposure D shown in Fig. 6 (a), and (b–e) tentative scenario how the structure may have formed as a result of four stages of brittle deformation and pseudotachylyte formation. Shortening inferred from restoration for fault veins 1, 2 and 3 probably represent minimum values. At each stage, the red dashed faults are the ones to become active in the next stage of faulting. Note that folding of fault veins 1 and 2 would require some slow ductile deformation prior to brittle faulting along faults 3 and 4. (For interpretation of the references to colour in this figure legend, the reader is referred to the Web version of this article.)

with an automated MAP 215–50 mass spectrometer in static mode, installed at the Geological Survey of Norway. The peaks and baseline (AMU = 36.2) were determined during peak hopping for 10 cycles (15 integrations per cycle, 30 integrations on mass ^{36}Ar) on the different masses ($^{41-35}$Ar) on a Balzers electron multiplier (SEV 217) and regressed back to zero inlet time. Samples C1A (1 and 2), D1B (3) and T1B (4) were analyzed on a SC 217 multiplier from MasCom. Blanks were analyzed every third measurement. After blank correction, a correction for mass fractionation, ^{37}Ar and ^{39}Ar decay and neutron-induced interference reactions produced in the reactor was undertaken using in-house software AgeMonster, written by M. Ganerød. This software implements the equations of McDougall and Harrison (1999) and the newly proposed decay constant for ^{4} K after Renne et al. (2011). A^{40}Ar/^{36}Ar ratio of 298.56 ± 0.31 from Lee et al. (2006) was used for the atmospheric argon correction and mass discrimination calculation using a power law distribution. We calculated J-values relative to an age of 28.608 ± 0.033 Ma (±σ) for the TCR sanidine flux monitor (Renne et al., 2011). Uncertainties are quoted at the 95% confidence level.

4.2. Results

Laser step heating results of the pseudotachylyte sample CdC14-20 from locality B are presented in Fig. 8a and Table 1. The step heating experiment yielded a weighted mean plateau age of 50.78 ± 0.23 Ma in the middle of the spectrum (Fig. 8a), accounting for 50.7% cumulative ^{39}Ar released, separated by older step ages at low and high temperatures of the experiment.

As mentioned above, we have supplemented our ^{40}Ar/^{39}Ar study of sample CdC14-20 with dating of pseudotachylyte samples from different localities along the shear zone (Fig. 1, exposures A, D and G, see also Figs. 9 and 10) and, together with sample CdC14-20 (Fig. 8a), the degassing spectra of these analyses are shown in Fig. 8b–e with corresponding age vs. Ca/K (calculated from $^{37}Ar_{Ca}/^{39}Ar_{K}$) plots. It should be noted that due to a detector error, some of the samples (C1A (1 and 2), D1B (3) and T1B (4)) were run after a long time since irradiation, making results less reliable since most of the ^{37}Ar produced from Ca has been decayed, precluding accurate calculation of Ca/K ratios and interference corrections. Except for sample T1A, all samples yield reproducible concordant segments, with early Eocene (Ypresian- Lutetian) ages. The apparent age vs. Ca/K ratios (Fig. 8a–e) diagrams clearly indicate that within-sample concordant steps, yielding early Eocene ages, come from mineral phase(s) with low Ca/K ratios, generally ≤0.5, which is compatible with degassing of matrix minerals, as reported for other natural pseudotachylytes (e.g., Zanchetta et al., 2011; Di Vincenzo et al., 2013, 2019). Results from sample T1A reported in Table 1 have been considered unreliable, possibly due to recoil effects or, more likely, to the presence of a higher portion of unmelted material from the source rock.

Aside that sample, however, our geochronological results clearly indicate that the Jurassic ductile shear fabric became overprinted by pseudotachylyte structures during the early Eocene. This calls for seismogenic reactivation along the intensely foliated, hence highly anisotropic shear zone structure during the Alpine orogeny.

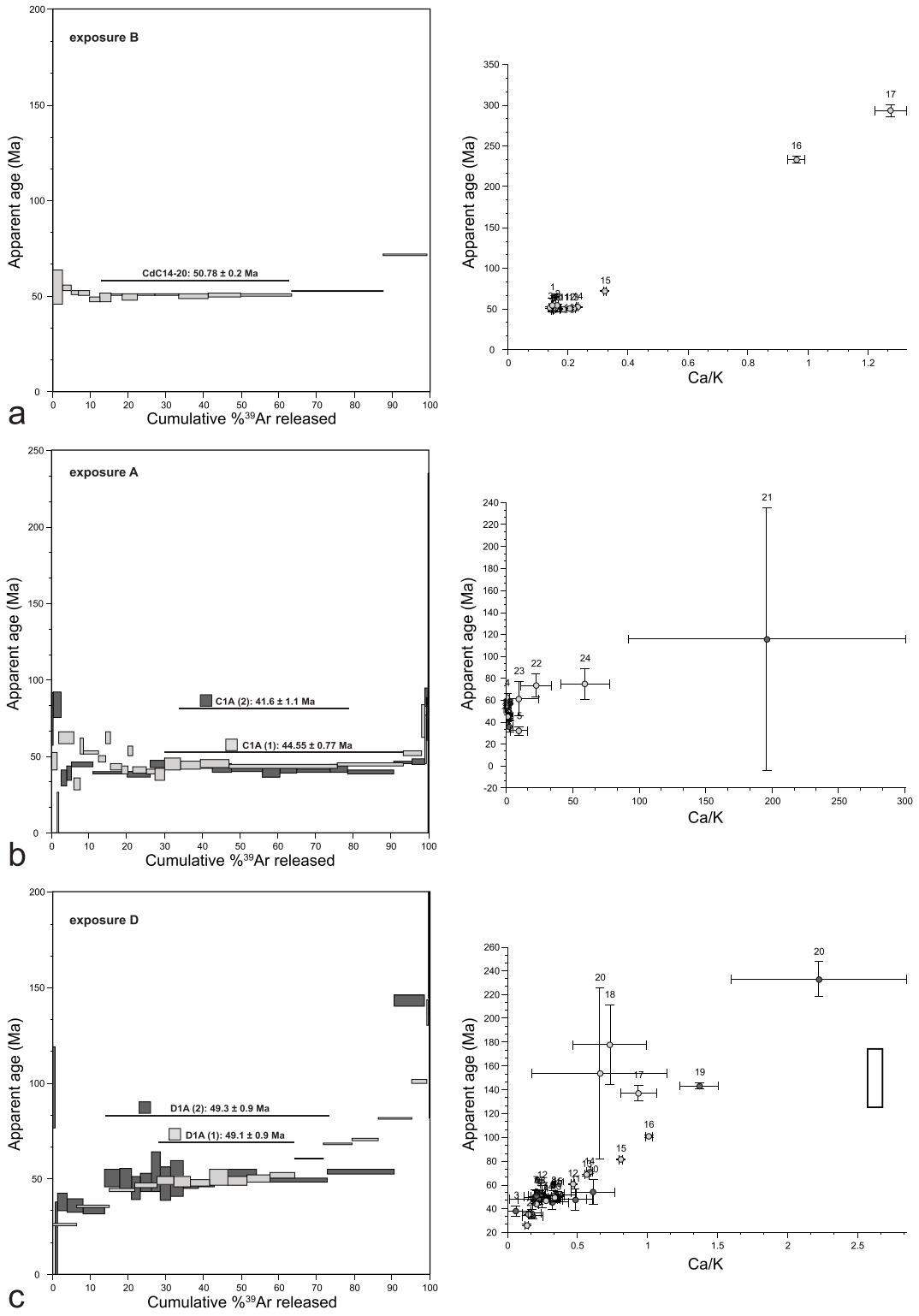

Fig. 8. Step heating release spectra of the pseudotachylyte samples dated in this study, with corresponding Ca/K vs. apparent age plots. Locations shown in Fig. 1 (a) Sample CdC14-20 from exposure B. (b) Samples C1A from exposure A. (c) Samples D1A from exposure D. (d) Samples D1B from exposure D. (e) Samples T1B from exposure G.

5. Discussion

Aside from our aim to document the pseudotachylyte structures and microstructures developed along the cala Culleró-Cala Fredosa shear zone, a first crucial aspect concerns the question whether or not the pseudotachylyte fault and injection veins result from frictional heating during coseismic motion along the pertinent fault surfaces. Secondly, the kinematics of the pseudotachylytes should be consistent with the history of Alpine shortening and strike-slip motion in the Pyrenean domain. Finally, the kinematic data, the size of the outcrop, and the

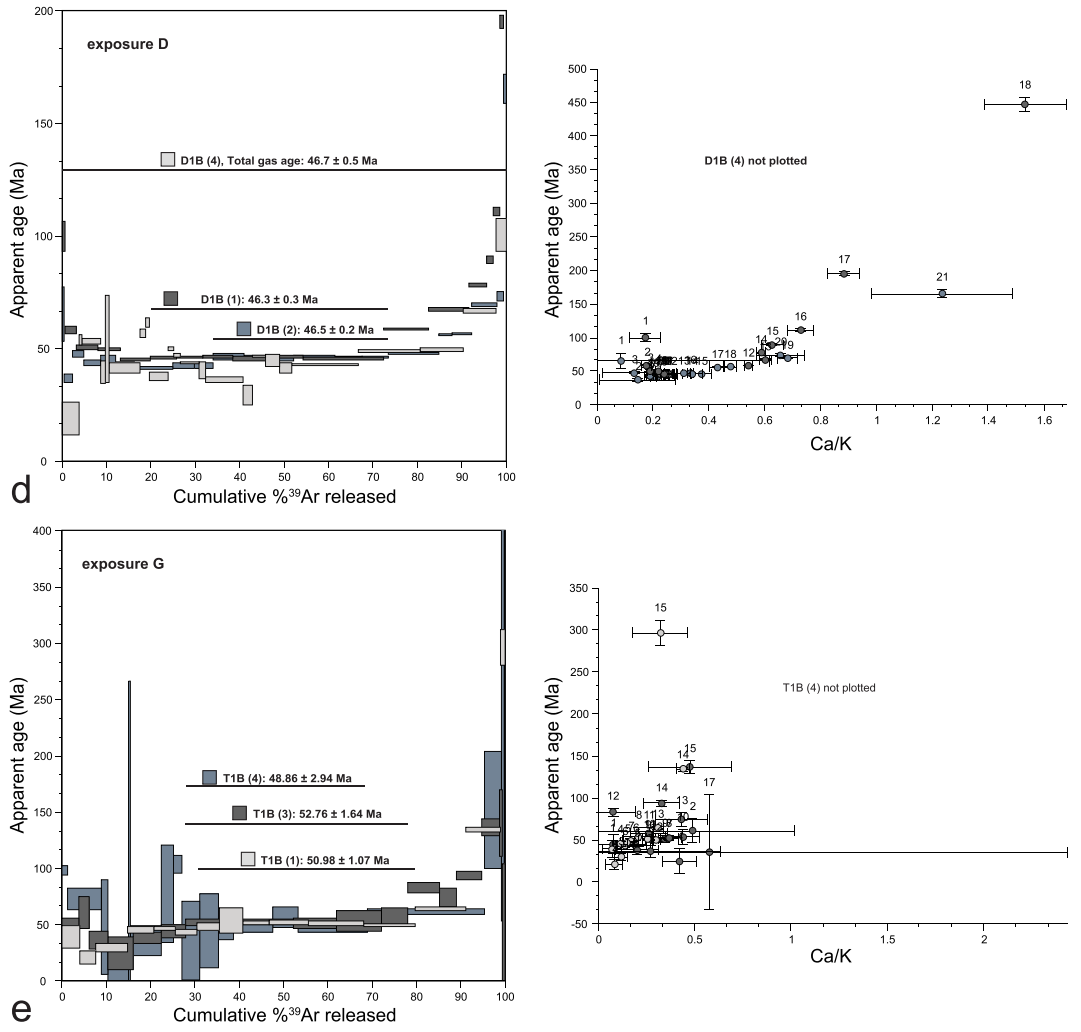

Fig. 8. (*continued*).

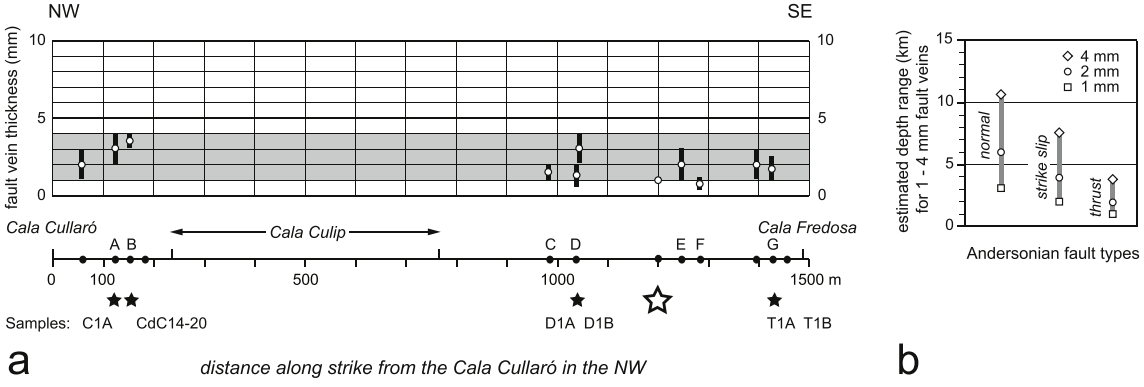

Fig. 9. (a) Fault vein thickness plotted against position along the Cala Cullaró – Cala Fredosa shear zone. Capital letters denote outcrops shown in Fig. 1 and referred to in text. Vein thicknesses have been measured on scaled field photographs and in thin sections. Bars indicate range of thickness per outcrop, mostly between 1 and 4 mm (grey shading), mean thickness per outcrop is indicated as white circle. The average thickness for all outcrops is ~2 mm. Black stars denote outcrops with dated pseudotachylytes, white star indicates location of dated shear fabric. (b) Estimated depths for 1–4 mm fault veins, assuming zero pore fluid pressure. Note that these depths differ for each of the Andersonian fault types.

thickness of the fault veins allow rough estimates of the associated earthquake source parameters and related energy budget. We now discuss these three aspects below.

5.1. Evidence for melting during coseismic frictional heating

Sibson and Toy (2006) list several criteria that pseudotachylytes should meet to possibly represent melt products of frictional heating. At the outcrop and hand specimen scale, these include fault vein - injection

Table 1
Main $^{40}Ar/^{39}Ar$ results.

Sample	Steps (n)	% 39Ar	Spectrum				Inverse Isochron			
			Age ± 1.96s	MSWD (P)	TGA ± 1.96s	K/Ca ± 1.96s	Age ± 1.96s	MSWD (P)	Trapped 40Ar/36Ar	Spread (%)
CdC14-20	6-13(8)	50.81	**50.78 ± 0.23**	0.56(0.79)	54.59 ± 0.32	5.88 ± 0.07	51.04 ± 0.97	0.61(0.72)	291.59 ± 14.30	17.6
C1A	16-20 (5)	63.36	**44.546 ± 0.770**	0.537(0.709)	46.521 ± 0.607	0.851 ± 1.026	43.982 ± 5.360	0.703 (0.550)	307.973 ± 94.475	9.5
C1A (2)	9-15(7)	47.16	41.587 ± 1.051	2.062(0.054)	43.565 ± 0.535	8.228 ± 114.365	**47.514 ± 3.315**	1.617 (0.152)	159.250 ± 93.978	5.1
D1A (2)	6-17 (12)	59.06	**49.344 ± 0.922**	1.495(0.125)	59.025 ± 0.777	3.372 ± 0.148	49.241 ± 1.418	1.609 (0.097)	306.214 ± 65.641	33.4
D1A (1)	5-10(6)	30	**49.089 ± 0.886**	0.735(0.597)	55.918 ± 0.375	2.985 ± 0.163	49.107 ± 3.908	0.917 (0.453)	298.385 ± 166.783	6.3
D1B (1)	6-11(6)	52.59	**46.289 ± 0.270**	1.252(0.282)	56.772 ± 0.237	4.024 ± 0.062	46.257 ± 0.739	1.538 (0.188)	305.789 ± 138.063	4
D1B (2)	10-15 (6)	39.44	**46.528 ± 0.202**	1.236(0.289)	48.614 ± 0.209	3.359 ± 0.121	46.699 ± 0.336	1.229 (0.296)	267.334 ± 54.627	5.7
D1B (3)	1-23 (23)	100	46.423 ± 2.217	131.438 (0.000)	**46.674 ± 0.479**	0.019 ± 0.005	NA			
T1B (1)	7-12(6)	49.14	**50.982 ± 1.069**	1.687(0.134)	58.041 ± 0.995	3.614 ± 0.125	46.941 ± 11.227	1.961 (0.097)	305.787 ± 21.320	4.9
T1B (3)	7-11(5)	50.21	**52.759 ± 1.642**	0.576(0.680)	58.640 ± 1.793	2.671 ± 0.230	55.745 ± 18.422	0.746 (0.524)	285.208 ± 94.475	5.7
T1B (4)	9-14(6)	41.94	**48.859 ± 2.940**	0.828(0.529)	59.058 ± 4.316		48.175 ± 15.314	1.036 (0.387)	303.379 ± 120.699	11
T1A (2)	11-16 (6)	39.95	**103.0 ± 0.6**	0.9(0.5)	111.9 ± 0.5	3.8 ± 0.1	103.2 ± 2.2	1.1(0.4)	285.6 ± 107.9	3.4
T1A (3)	1-14 (14)	100	163.910 ± 4.815	258.410 (0.000)	**165.867 ± 0.367**	3.564 ± 0.043	289.465 ± 112.770	32.200 (0.000)	−8172.546 ± 25021.159	44.1
T1A	15-17 (3)	15.3	120.925 ± 0.171	1.114(0.328)	**154.110 ± 0.170**	4.348 ± 0.042	120.814 ± 2.274	2.214 (0.000)	302.096 ± 72.712	2

Annotations in the table are as follows: TGA = total gas age, MSWD (P) is the mean squared weighted deviations and probability of fit, spread is the spread along the isochron line (Jourdan et al., 2009). Uncertainties are reported as analytical errors quoted at the 1.96σ level. Analyses from sample T1A yielded older ages due to recoil effects or, more likely, because of a higher proportion of unmelted material from the source rock in the matrix. The Total Gas Age (like K–Ar) is in line with the remaining samples. In sample C1A(2) the trapped $^{40}Ar/^{36}Ar$ indicates loss of ^{40}Ar, so we use the inverse isochron age.

vein geometries, markedly sharp boundaries of the veins with the host rock, a zonal colour banding possibly reflecting chilled margins, no grains visible with naked eye in matrix, embayed clasts, and a glassy luster and/or conchoidal fracture surface of the veins. At the microscale, criteria such as embayed clasts, microcrystallites/spherulites, variation of microcrystallite texture at vein margins, dendritic crystal habits, sulphide droplets, and the microstructure of injection veins may all indicate the former existence of a melt. A convincing argument in favour of a former melt phase is the presence of glass, but in geologically non-recent pseudotachylytes such glasses may well have devitrified and recrystallized.

The pseudotachylyte exposures at Cap de Creus are characterized by fault and injection veins of cryptocrystalline material, by the markedly sharp boundaries of the dark-coloured veins and, occasionally, a glassy luster and conchoidal fracture surfaces. These features all suggest that the exposed pseudotachylyte material did indeed form from a melt. At the microscale, embayed clasts and occasional millimetre-scale isoclinal folds seem consistent with flow of an essentially fluid (liquid) phase, and this also applies to the shape preferred orientation of tiny clasts such as in Fig. 4b that could have developed during flow of a matrix melt. The most convincing evidence, however, is the clearly igneous, microporphyritic microstructure of the pseudotachylyte matrix at the 10 ?m scale and smaller, seen in at least two of the dated pseudotachylytes from the Cala Cullaró peninsula, and made up of non-oriented biotite and feldspar and enclosing ultrafine clasts of quartz. The mineral composition of this matrix is also consistent with the essentially pelitic composition of the sheared protolith as follows. As emphasized by Spray (2010), the development of frictional melts is a nonequilibrium process involving initial cataclastic grain size reduction, comminution and subsequent melting, affecting first the low hardness sheet silicates with rather low individual melting points, followed by harder feldspars with higher melting points, and eventually leaving quartz as clasts. The country rock minerals thus melt in a sequence controlled by their mechanical properties and individual melting points. Given the phyllosilicate-rich composition of the mylonitic country rock, a more ferromagnesian, biotite-rich melt can be expected which, owing to its low viscosity, has an enhanced potential to act as a lubricant. All of the observational evidence from the pseudotachylyte structures and microstructures in the Cala Cullaró – Cala Fredosa shear zone thus seem consistent with the former presence of a melt phase in fault and injection veins, presumably generated during coseismic frictional melting.

5.2. *Kinematics of the pseudotachylytes in the context of the Alpine orogeny*

We now turn to the tectonic setting of the pseudotchylyte-forming process during Alpine reactivation. The orientation data for the ductile and pseudotachylyte structures are summarized in Fig. 11a and b. Note that the ductile stretching direction is subhorizontal on a NE dipping shear plane (Fig. 11a), and that the lineations on fault veins have similar orientations (Fig. 11b). Kinematic criteria consistently indicate subhorizontal ductile shearing with a dextral, top-to-the-SE sense of motion, whilst the movement direction of the pseudotachylyte is subhorizontal but with an opposite, top-to-the-NW sense

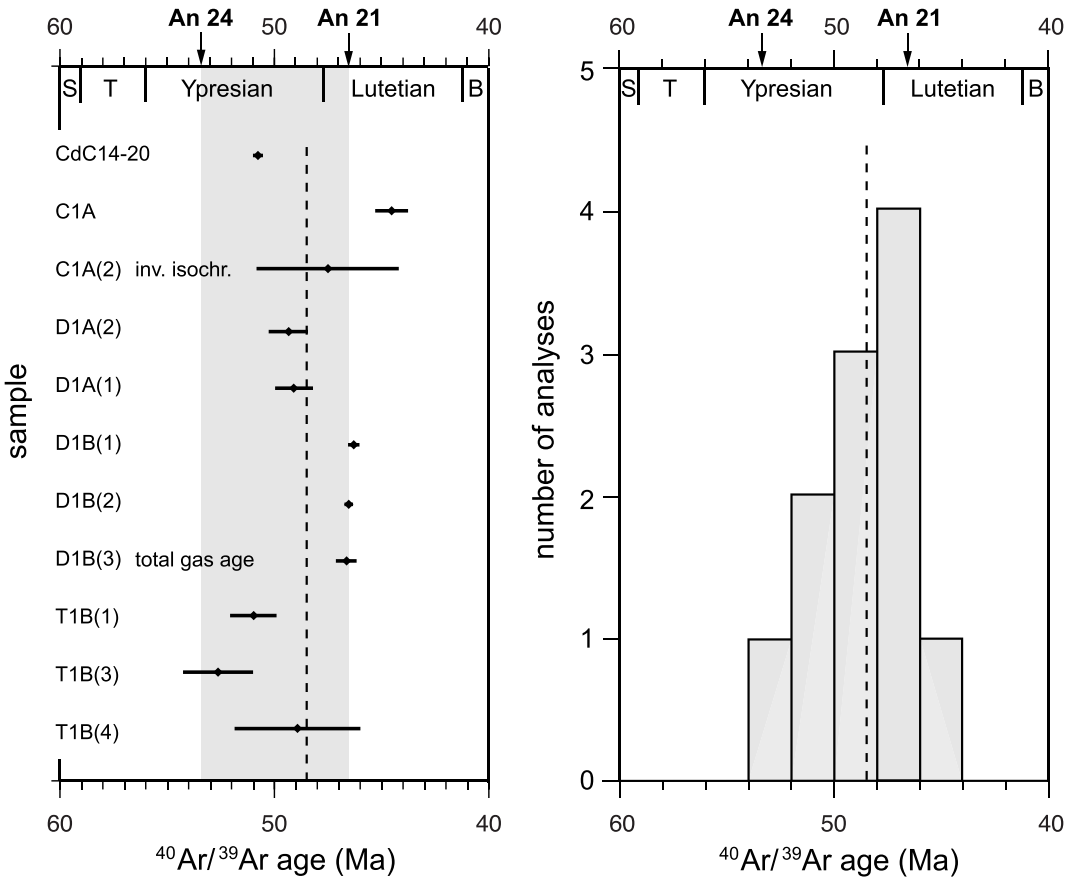

Fig. 10. $^{40}Ar/^{39}Ar$ age results obtained in five samples of the Cala Cullero - Cala Fredosa pseudotachylytes. Left panel shows ages with uncertainties, samples correspond to those shown in Table 1. Right panel shows histogram representing 11 analyses obtained from the five samples. Except for samples C1A and D1B, all $^{40}Ar/^{39}Ar$ ages plot in between An 24 and An 21. Abbreviations: S, Selandian; T, Thanetian; B, Bartonian.

(Fig. 11b). The Variscan basement rocks of Cap de Creus form part of the Iberian margin presently preserved south of the North Pyrenean Fault (Fig. 11c). The Iberian margin was affected by Alpine continental collision of Iberia and Eurasia from the latest Cretaceous till the Miocene. The collisional process resulted in a minimum cumulative shortening of some 165 km, evidenced from restoration of the deep seismic ECORS Pyrenees section (Beaumont et al., 2000), during which time the original Jurassic shear zones, and the attenuated Variscan metamorphic field gradient, became likely tilted northwards by ~90° towards their modern orientation (Vissers et al., 2017). Whilst the net shortening direction is approximately N–S, plate kinematic reconstructions (Vissers and Meijer, 2012) show that the shortening direction varied considerably with time. The well-confined early Eocene (Ypresian-Lutetian) ages of the pseudotachylytes (between 52.76 ± 1.64 Ma and 44.55 ± 0.77 Ma, see Table 1), allow interpretation of the associated brittle strike-slip deformation against the background of Iberian plate kinematics. Based on ocean floor magnetic anomaly fitting in a six-plate circuit, Euler poles for Iberia with respect to Europe for anomaly (chron) An24 (53.3015 Ma) and An21 (46.536 Ma) describe the positions of Iberia shortly before and during the main stages of pseudotachylyte development (Figs. 10 and 11c). From this reconstruction, and using the stage pole describing the motion of Iberia from chron 24 to chron 21, an average shortening direction can be calculated trending WNW-ESE, i.e., clearly different from the cumulative NS directed shortening of the Pyrenees, but remarkably consistent with brittle reactivation along a NW-trending shear zone and development of pseudotachylyte fault veins with top-to-the-NW kinematics (Fig. 11c).

5.3. Earthquake source parameters and energy density allied with the fault veins

5.3.1. Seismic moment

With the notion that the pseudotachylyte fault veins at Cap de Creus may have formed in response to coseismic faulting, the displacements (~25 and 40 cm) needed to form the duplex structure at locality D should be a measure of coseismic slip. We note, however, that it is unclear if the pseudotachylyte fault veins all developed during one single event, or if these different slips represent different earthquakes. We also note that the observed displacements are not necessarily equal to the mean values of coseismic slip.

The mapped outcrop of the pseudotachylyte-bearing shear zone is 1500 m long, and at both ends the structure likely continues below sea level. Together with the slip values, we may estimate the associated earthquake magnitude because both the dimensions of the fault and the slip value are parameters contributing to the seismic moment (Mo):

$$Mo = \mu A \overline{D} \quad (1)$$

where ? is the shear modulus, A the rupture surface and $\overline{D}$ the average displacement (slip) along the fault. A lower bound to the rupture surface A can be estimated via the exposed length of the pseudotachylyte bearing shear zone assuming a circular slipped area of $?r^2$ representing a reasonable minimum value of A with a radius r = 750 m. For an average displacement of 0.25 m and a shear modulus of 30 GPa, Mo = 1.32 × 10^{16} Nm, yielding a moment magnitude Mw of 4.75 (Hanks and Kanamori, 1979). For a slip value of 0.40 m, Mo = 2.12 × 10^{16} Nm, which is equivalent to Mw = 4.88.

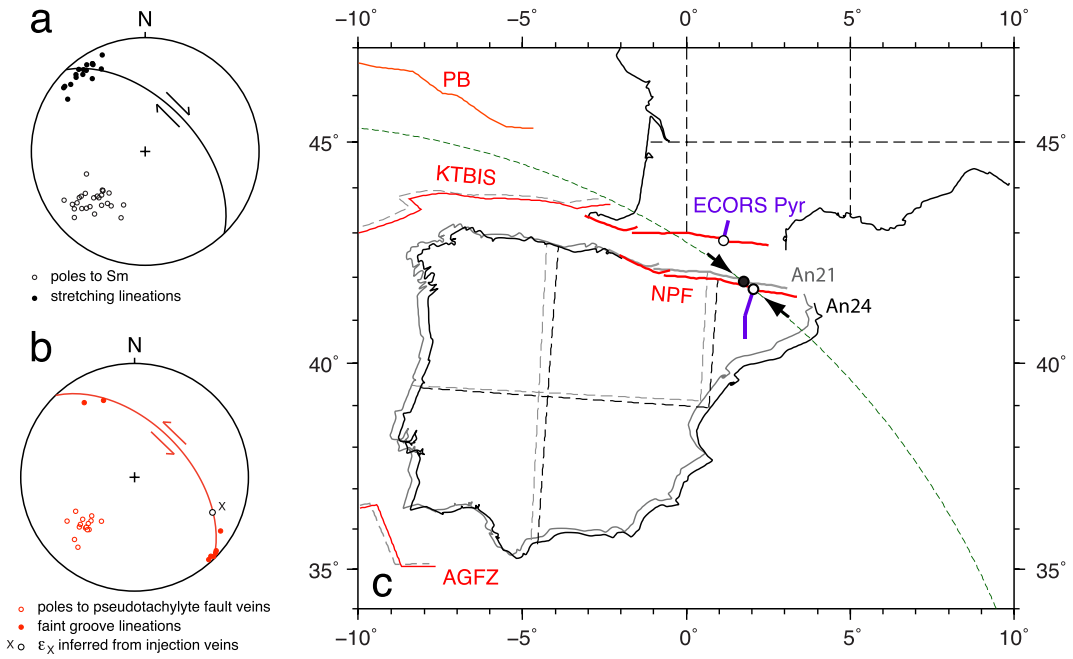

Fig. 11. Cumulative orientation data for all pseudotachylyte-bearing outcrops studied (equal area, lower hemisphere projection). (a) Greenschist facies mylonitic structures, greatcircle denotes average orientation of mylonitic foliation. (b) Orientation data for pseudotachylyte structures, greatcircle denotes average orientation of fault veins. (c) Reconstructed positions of Iberia with respect to Europe for anomaly An 24 (black, 53.3015 Ma) and An 21 (grey, 46.536 Ma), after Vissers and Meijer (2012). AGFZ, Azores Gibraltar Fracture Zone; KTBIS, King's Trough-Biscay boundary; NPF, North Pyrenean Fault; PB, Porcupine boundary. Deformation in the Pyrenean domain affected the passive margins of Europe and Iberia, but are shown in the restoration as a displacement of the North Pyrenean Fault (NPF) and a markerpoint at the intersection of the NPF with the ECORS Pyrenees seismic section. Note that most of the $^{40}Ar/^{39}Ar$ ages of the Cap de Creus pseudotachylytes plot in between An 24 and An 21. Dashed small circle denotes stage-pole motion of the markerpoint at that stage (white towards black) indicating shortening at a high angle to the overall NS directed shortening of the belt.

5.3.2. Fault vein thickness, shear resistance and energy dissipation

The observed fault vein thicknesses in the Cap de Creus pseudotachylytes allow estimates of the average shear resistance during slip $\overline{\tau}_F$ via the energy dissipated to form the melt layers by coseismic frictional melting. Such analysis by Di Toro et al. (2005) and Sibson and Toy (2006) shows that for adiabatic melting from frictional dissipation the thickness t of the melt layer can be approximated by:

$$t = Q \Big/ \rho E_m \quad \text{where } Q = \overline{\tau}_F D \text{ and } E_m = c_p(T_m - T_a) + \Delta h_{fus}(1 - \phi) \qquad (2)$$

where Q is the frictional heat generated per unit area of the fault, ρ the rock density, and E_m the energy per unit mass needed to melt the host rock. $\overline{\tau}_F$ is the average shear resistance during slip, D the coseismic displacement, whilst the parameters to calculate E_m are c_p the specific heat, T_m the melting temperature, T_a the ambient host rock temperature at the onset of slip, Δh_{fus} the latent heat of fusion, and ϕ the proportion of unmelted clasts. From equation (2) it follows that (see also Di Toro et al., 2005):

$$\overline{\tau}_F = t\rho E_m / D \qquad (3)$$

whilst the energy dissipation per unit area of a fault surface to form a frictional melt layer of thickness t is:

$$Q = t\rho E_m \qquad (4)$$

Fault vein thicknesses observed at Cap de Creus are between 1 and 4 mm, and often vary even on the outcrop scale. Fig. 9a shows vein thicknesses in 11 exposures along the host shear zone, measured using field photographs and thin sections. The average of the mean values per exposure (white dots) along the shear zone is ~2 mm. We therefore estimate the average shear resistance $\overline{\tau}_F$ associated with 2 mm thick fault veins for coseismic displacements D = 0.25 m and D = 0.40 m. Apart from fault vein thickness and displacement values, $\overline{\tau}_F$ is also a function of E_m and therefore of host rock temperature prior to slip which, unfortunately, is poorly constrained. In view of the Jurassic $^{40}Ar/^{39}Ar$ age of the host shear zone, T_a must have been below the $^{40}Ar/^{39}Ar$ closure temperature for muscovite (~350 °C). Exhumation studies in the central Pyrenees (e.g, Sinclair et al., 2005) indicate ongoing erosion of the Axial Zone already in the Early Eocene suggesting that also at Cap de Creus ambient temperatures may have been substantially lower than 350 °C in response to erosional exhumation of the thickening crust, although the $^{40}Ar/^{39}Ar$ white mica age of 58.57 ± 0.55 from another ductile shear zone in Cap de Creus (Vissers et al., 2017) indicates that those sheared rocks may still have been at lower greenschist-facies conditions. We therefore explore $\overline{\tau}_F$ for ambient host rock temperatures T_a of 100 and 300 °C, and use ρ = 2650 kg/m3, c_p = 1200 J/kg°C, a melting temperature of 1200 °C, Δh_{fus} = 500 kJ/kg, and ? = 0.2. Our choice for the value of c_p is corroborated by the average composition of the host shear zone rocks, whilst the pseudotachylyte microstructures indicate that a proportion ϕ = 0.2 of clasts in the matrix is reasonable. For a 2 mm melt layer, the average shear resistance $\overline{\tau}_F$ calculated for 0.25 m slip and T_a = 100 °C is 36.5 MPa, whilst T_a = 300 °C yields 31.4 MPa. For 0.4 m slip, these values are 22.8 and 19.6 MPa, respectively. The associated energy dissipation is 9.1 MJ/m^2 for T_a = 100 °C, and 7.8 MJ/m^2 for T_a = 300 °C. Like Sibson and Toy (2006) we find that the energy dissipation on a fault surface to form melt layers 1 and 10 mm thick is ~4.5 and ~45 MJ/m^2.

Bearing in mind that the kinematics of the fault veins at Cap de Creus indicate brittle strike-slip reactivation of a moderately to steeply dipping anisotropic shear zone, we infer that the fault veins are best described as strike-slip structures. We therefore use estimates of the depth-dependent frictional shear strength on optimally oriented faults by Sibson and Toy (2006) for the case of strike-slip faulting, but also explore normal and thrust faults. Note that the temperature increase during melting ($T_m - T_a$) is also depth-dependent because the ambient host rock temperature T_a increases with depth along the geotherm, hence that ($T_m - T_a$) decreases with increasing depth. It follows that, for each of the main

Andersonian fault types, a given fault vein thickness also serves to model the coeval depth of the fault zone. Like Sibson and Toy (2006) we make the assumption that ?$_F$ drops linearly to zero during slip, so that the average kinetic resistance is half the initial static frictional strength, and perform our calculations for a dry crust, i.e., for zero pore fluid pressure. Note again that the depths at which melt veins of a given thickness are expected to form vary with Andersonian fault type (Fig. 9b). For a strike slip fault, 2 mm thick fault veins are inferred to form at a depth of ~4 km, but note that any pore fluid pressure would result in larger depth values hence that the inferred depth must be considered a minimum value.

5.3.3. Energy dissipation and apparent stress estimates from seismology

The estimated energy dissipation for 1, 2, and 10 mm melt layers is shown in the diagram of Fig. 12 modified after Sibson and Toy (2006). This allows comparison with seismological estimates of earthquake fracture energy ranging from 0.1 to 10 MJ/m^2 (Abercrombie and Rice, 2005) shown in grey shading. The diagonal shear stress contours define combinations of slip and average frictional resistance that could give rise

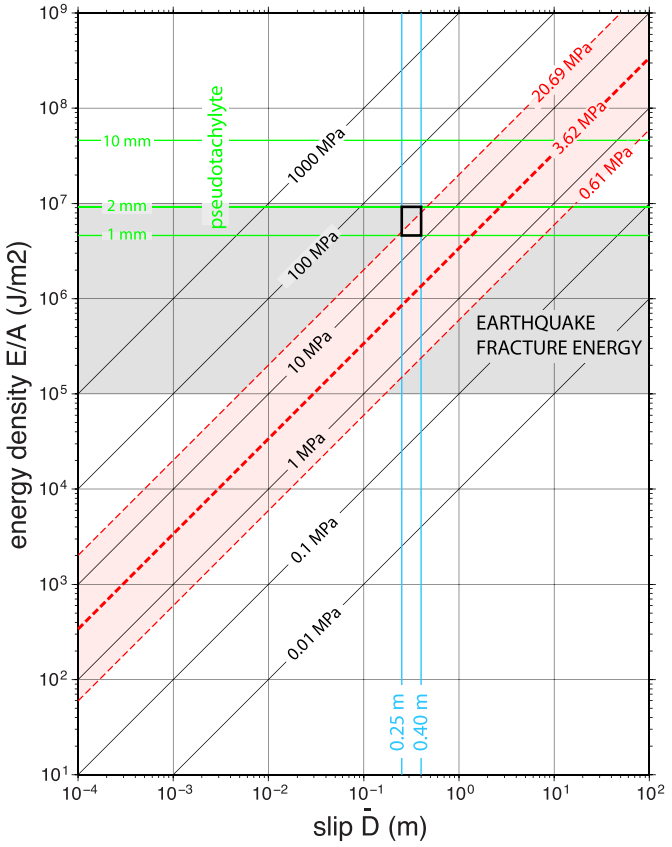

Fig. 12. Energy density per square meter of fault surface versus average slip ($\overline{D}$), modified after Sibson and Toy (2006). Common values of earthquake fracture energy outlined in grey shading, for comparison with the energy required to produce pseudotachylyte melt layers of various thickness by adiabatic dissipation shown in green for 1, 2 and 10 mm thick fault veins. Diagonal shear stress contours relate energy dissipation to earthquake slip for average values of frictional resistance, but also define the radiated wave energy density in relation to slip for different values of apparent stress. Lightred field denotes range of apparent stresses associated with strike-slip earthquakes after Choy and Boatwright (1995), with an average value of 3.62 MPa (thick dashed line) and 95% lower and upper bounds at 0.61 and 20.69 MPa. Rectangle defined by fault vein thicknesses of 1–2 mm and slip values of 0.25–0.40 m documented in this study from the Cap de Creus pseudotachylytes partly overlaps with the range of apparent stresses of strike-slip earthquakes at ~20 MPa. (For interpretation of the references to colour in this figure legend, the reader is referred to the Web version of this article.)

to melt layers of different thickness. As noted by Sibson and Toy (2006), they also represent contours of apparent stress relating radiated wave energy per unit area of the fault to displacement. Apparent stress (Wyss and Brune, 1968) of an earthquake (the product of seismic efficiency, η, and the average shear stress over the fault surface during slip, $\overline{\tau}$? is defined as:

$$\tau_a = (\eta\overline{\tau}) = \mu(E_r / \mathrm{Mo}) \quad (5)$$

where E_r is the radiated wave energy, Mo the seismic moment, and μ the shear modulus. As $MO = \mu A\overline{D}$ (equation (1)), this can be rewritten as:

$$\tau_a = E_r/(A\overline{D}) \quad (6)$$

so that apparent stress is the wave energy radiated per square meter of the fault surface, per meter displacement. Values for apparent stress commonly lie in the range 0.1–1 MPa, equivalent to 0.1–1 MJ/m^2 of radiated wave energy per meter displacement (Pérez-Campos and Beroza, 2001), with an apparent upper limit for continental earthquakes at 10 MPa (McGarr and Fletcher, 2003). From the diagram of Fig. 12 it is clear that 1–10 mm pseudotachylyte melt layers would require seismic displacements of centimeters to decimeters when $\overline{\tau}_F$ ~100 MPa, in comparison with displacements of decimeters to meters when $\overline{\tau}_F$ ~10 MPa. Choy and Boatwright (1995), however, have shown that the apparent stress of strike-slip earthquakes is significantly higher, with a mean value of 3.62 MPa and a 95% geometric spread between 0.61 and 20.69 MPa, which may be pertinent to the case of the Cap de Creus pseudotachylytes indicating subhorizontal slip. Pérez-Campos and Beroza (2001) also conclude that the apparent stresses of strike-slip earthquakes are larger than those of normal and thrust faults, but smaller than those estimated by Choy and Boatwright (1995). The apparent stress values for strike-slip earthquakes of Choy and Boatwright (1995) are shown in Fig. 12 (red shading). The displacements of 0.25–0.40 m and the energy density for 1–2 mm fault veins define a rectangular field that overlaps with the high 95% boundary of Choy and Boatwright (1995), whilst a 2 mm fault vein formed at 0.40 m slip requires $\overline{\tau}_F = 22.8$ MPa, i.e. slightly larger than the upper 95% boundary of 20.69 MPa. A seismogenic origin of the Cap de Creus pseudotachylytes seems thus in reasonable agreement with studies of strike-slip earthquakes in seismology.

5.3.4. Earthquake source parameters and geological constraints

Our calculations suggest that the pseudotachylytes may have formed in response to one or more strike-slip earthquakes at a minimum depth of ~4 km, with a seismic moment in the range of 1.3×10^{16} to 2.1×10^{16} Nm (Mw ~ 4.7–4.9), and an average frictional resistance of ~23 MPa. This raises the question what the coeval overburden was now removed by erosion. The thickness of the Paleozoic sequence and possibly overlying Mesozoic and lower Cenozoic rocks is difficult to estimate. Castiñeiras et al. (2008) describe an upper Proterozoic - lower Paleozoic stratigraphy at Cap de Creus of 2600 m, at nearby Roc de Frausa of 4260 m and, farther to the west at Canigou, of 4550 m. The Mesozoic is not exposed in the easternmost Pyrenees, but Vergés et al. (1995) document a Mesozoic-Paleocene succession in the eastern Pyrenees of 3000–5000 m. The total overburden at Cap de Creus may thus have been about 8 km, but the present day geology only accounts for some 2.5 km of upper Proterozoic - lower Paleozoic metasediments and Variscan granitoids (Carreras, 2001) because Alpine uplift and erosion removed much of the Paleozoic and possibly Mesozoic rocks. However, the thickness of these rocks in the nearby areas to the west suggests that during the Cenozoic an overburden of more than 4 km as inferred in our calculations is reasonable.

6. Conclusions

A greenschist facies shear zone transecting amphibolite-facies metasediments and associated pegmatites at the Cap de Creus peninsula

contains pseudotachylytes characterized by up to 4 mm thick fault veins and cm-scale high-angle injection veins. Microstructural study of the pseudotachylyte reveals ultrafine-grained domains (down to a few micrometers) of biotite and feldspar with a clearly igneous, microporphyritic structure suggesting crystallization from a melt. This observation lends support to an interpretation of the pseudotachylytes as the product of coseismic frictional melting.

Recent $^{40}Ar/^{39}Ar$ dating of the shear zone rocks have revealed a Jurassic (~162 Ma) age for the mylonites. Here we present results of an $^{40}Ar/^{39}Ar$ study of the pseudotachylytes yielding Early Eocene (Alpine) ages between 52.76 ± 1.64 Ma and 44.55 ± 0.77 Ma. In addition, albeit surrounded with some uncertainties, the kinematics of the pseudotachylyte structures suggest a top-to-the-NW sense of motion, i.e. opposite to the sense of shear in the surrounding shear zone rocks. Both the geometry and kinematics of the pseudotachylytes and their age suggest seismogenic brittle reactivation of the earlier shear zone structure during the Alpine orogeny. Reactivation likely post-dated tilting of Jurassic low-angle normal shearzones, and involved brittle strike-slip motions. This fits well with a coeval stage of strike-slip motion between Iberia and Europe inferred from magnetic anomaly-based plate kinematic reconstructions.

The dimensions of the pseudotachylyte-bearing shear zone and estimates of the displacement of 0.25–0.40 m along the fault veins point to minimum values of the associated seismic moment Mo of 1.3×10^{16} to 2.1×10^{16} Nm, equivalent with a moment magnitude Mw of ~4.7–4.9. The average thickness of the fault veins is ~2 mm, and given their strike-slip kinematics this suggests that they may have formed at 4 km depth, at an energy density of $\sim 9 \times 10^6$ J/m^2 and an average frictional resistance of ~23 MPa, i.e. slightly higher than the apparent stresses of strike-slip earthquakes documented in seismological studies.

CRediT authorship contribution statement

Reinoud L.M. Vissers: Conceptualization, Writing - original draft, Writing - review & editing. **Morgan Ganerød:** Formal analysis, Methodology, Writing - review & editing. **Gill M. Pennock:** Formal analysis. **Douwe J.J. van Hinsbergen:** Conceptualization, Funding acquisition, Writing - original draft, Writing - review & editing.

Acknowledgements

We are indebted to Martyn Drury, Chris Spiers, Colin Peach, Tim Wolterbeek and Bart Verberne for their continuous interest and discussion of the Cap de Creus pseudotachylytes and their significance. A challenging and constructive review by Virginia Toy of an earlier version of this paper led to considerable improvement. Exchange of ideas with André Niemeijer and Giulio di Toro was very helpful and encouraging. We are indebted to Florian Fusseis and Gianfranco Di Vincenzo for their critical comments. DJJvH acknowledges funding through NWO Vici grant 865.17.001.

Appendix A. Supplementary data

Supplementary data related to this article can be found at https://doi.org/10.1016/j.jsg.2020.103994.

References

Abercrombie, R.E., Rice, J.R., 2005. Can observations of earthquake scaling constrain slip weakening? Geophys. J. Int. 162, 406–424. https://doi.org/10.1111/j.1365-246X.2005.02579.x.

Beaumont, C., Muñoz, J.A., Hamilton, J., Fullsack, P., 2000. Factors controlling the alpine evolution of the central Pyrenees inferred from a comparison of observations and geodynamical models. J. Geophys. Res. 105, 8121–8145.

Carreras, J., 2001. Zooming on northern Cap de Creus shear zones. J. Struct. Geol. 23, 1457–1486.

Carreras, J., Estrada, A., White, S., 1977. The effects of folding on the c- axis fabrics of a quartz-mylonite. Tectonophysics 39, 3–24.

Carreras, J., Julivert, M., Santanach, P., 1980. Hercynian Mylonite Belts in the Eastern Pyrenees: an example of shear zones associated with late folding. J. Struct. Geol. 2, 5–9.

Castiñeiras, P., Navidad, M., Liesa, M., Carreras, J., Casas, J.M., 2008. U–Pb zircon ages (SHRIMP) for Cadomian and Early Ordovician magmatism in the Eastern Pyrenees: new insights into the pre-Variscan evolution of the northern Gondwana margin. Tectonophysics 461, 228–239. https://doi.org/10.1016/j.tecto.2008.04.005.

Choy, G.L., Boatwright, J.L., 1995. Global patterns of radiated seismic energy and apparent stress. J. Geophys. Res. 100, 18205–18228.

Di Toro, G., Pennacchioni, G., Teza, G., 2005. Can pseudotachylytes be used to infer earthquake source parameters? An example of limitations in the study of exhumed faults. Tectonophysics 402, 3–20.

Di Vincenzo, G., Rocchi, S., Rossetti, F., Storti, F., 2004. ^{40}Ar-^{39}Ar dating of pseudotachylyites: the effect of clast-hosted extraneous argon in Cenozoic fault-generated friction melts from the West Antarctic Rift System. Earth Planet Sci. Lett. 223, 349–364.

Di Vincenzo, G., Rossetti, F., Viti, C., Balsamo, F., 2013. Constraining the timing of fault reactivation: Eocene coseismic slip along a Late Ordovician ductile shear zone (northern Victoria Land, Antarctica). Geol. Soc. Am. Bull. 125, 609–624.

Di Vincenzo, G., Pennacchioni, G., Bestmann, M., 2019. Exloring the Argon isotope record of an early Miocene pseudotachylyte in an early Oligocene intrusion (Rieserferner pluton, eastern Alps). Lithos 338–339, 1–17.

Druguet, E., 1997. The structure of the NE Cap de Creus peninsula. Relationships with metamorphism and magmatism. PhD thesis. Universitat Autonoma de Barcelona.

Druguet, E., Castro, A., Chichorro, M., Francisco Pereira, M., Fernández, C., 2014. Zircon geochronology of intrusive rocks from Cap de Creus, Eastern Pyrenees. Geol. Mag. 151, 1095–1114.

Druguet, E., Passchier, C.W., Carreras, J., Victor, P., den Brok, S., 1997. Analysis of a complex high-strain zone at Cap de Creus, Spain. Tectonophysics 280, 31–45.

Etheve, N., Mohn, G., Frizon de Lamotte, D., Roca, E., Tugend, J., Gómez-Romeu, J., 2018. Extreme mesozoic crustal thinning in the eastern Iberia margin: the example of the columbrets basin (valencia trough). Tectonics 37, 636–662.

Fusseis, F., Handy, M.R., Schrank, C.E., 2006. Networking of shear zones at the brittle-to-viscous transition (Cap de Creus, NE Spain). J. Struct. Geol. 28, 1228–1243.

Fusseis, F., Handy, M.R., 2008. Micromechanisms of shear zone propagation at the brittle–viscous transition. J. Struct. Geol. 30, 1242–1253.

Grocott, J., 1981. Fracture geometry of pseudotachylyte generation zones: a study of shear fractures formed during seismic events. J. Struct. Geol. 3, 169–178.

Hanks, T.C., Kanamori, H., 1979. A moment magnitude scale. J. Geophys. Res. 84, 2348–2350.

Jourdan, F., Renne, P.R., Reimold, W.U., 2009. An appraisal of the ages of terrestrial impact structures. Earth Planet Sci. Lett. 286, 1–13.

Kirkpatrick, J.D., Shipton, Z.K., Persano, C., 2009. Pseudotachylytes: rarely generated, rarely preserved of rarely reported? Bull. Seismol. Soc. Am. 99, 382–388.

Lee, J.Y., Marti, K., Severinghaus, J.P., Kawamura, K., Yoo, H.S., Lee, J.B., Kim, J.S., 2006. A redetermination of the isotopic abundances of atmospheric. Ar. Geochim. Cosmochim. Acta 70, 4507–4512.

Magloughlin, J.F., 1992. Microstructural and chemical changes associated with cataclasis and frictional melting at shallow crustal levels: the cataclasite-pseudotachylyte connection. Tectonophysics 204, 243–260.

McDougall, I., Harrison, T.M., 1999. Geochronology and Thermochronology by the $^{40}Ar/^{39}Ar$ Method. Oxford University Press, New York.

McGarr, A., Fletcher, J.B., 2003. Maximum slip in earthquake fault zones, apparent stress, and stick-slip friction. Bull. Seismol. Soc. Am. 93, 2355–2362.

Passchier, C.W., 1982. Pseudotachylyte and the development of ultramylonite bands in the saint-barthélemy Massif, French Pyrenees. J. Struct. Geol. 4, 69–79.

Passchier, C.W., 1984. The generation of ductile and brittle shear bands in a low-angle mylonite zone. J. Struct. Geol. 6, 273–281.

Pennacchioni, G., Di Toro, G., Brack, P., Menegon, L., Villa, I.M., 2006. Brittle-ductile-brittle deformation during cooling of tonalite (Adamello, southern Italian Alps). Tectonophysics 427, 171–197.

Pérez-Campos, X., Beroza, G.C., 2001. An apparent mechanism dependence of radiated seismic energy. J. Geophys. Res. 106, 11127–11136.

Platt, J.P., Vissers, R.L.M., 1981. Extensional structures in anisotropic rocks. J. Struct. Geol. 2, 397–410.

Renne, P.R., Balco, G., Ludwig, K.R., Mundil, R., Min, K., 2011. Response to the comment by W.H. Schwarz et al. on "Joint determination of ^{40}K decay constants and $^{40}Ar^*/^{40}K$ for the Fish Canyon sanidine standard, and improved accuracy for $^{40}Ar/^{39}Ar$ geochronology" by P.R. Renne et al (2010). Geochem. Cosmochim. Acta 75 (17), 5097–5100. https://doi.org/10.1016/j.gca.2011.06.02.

Sherlock, S.C., Watts, L.M., Holdsworth, R.E., Roberts, D., 2004. Dating fault reactivation by Ar/Ar laserprobe: an alternative view of apparently cogenetic mylonite – pseudotachylite assemblages. J. Geol. Soc. Lond. 161, 335–338.

Sherlock, S.C., Strachan, R.A., Jones, K.A., 2009. High spatial resolution $^{40}Ar/^{39}Ar$ dating of pseudotachylites: geochronological evidence for multiple phases of faulting within basement gneisses of the Outer Hebrides (UK). J. Geol. Soc. Lond. 166, 1049–1059. https://doi.org/10.1144/0016-76492008-125.

Sibson, R.H., 1977. Fault rocks and fault mechanisms. J. Geol. Soc. Lond. 133, 191–213.

Sibson, R.H., 1980. Transient discontinuities in ductile shear zones. J. Struct. Geol. 2, 165–171.

Sibson, R.H., 1983. Continental fault structure and the shallow earthquake source. J. Geol. Soc. Lond. 140, 741–767.

Sibson, R.H., Toy, V.G., 2006. The habitat of fault-generated pseudotachylyte: presence vs. absence of friction-melt. AGU Geophys. Monograph 170, 153–166.

Sinclair, H.D., Gibson, M., Naylor, M., Morris, R.G., 2005. Asymmetric growth of the Pyrenees revealed through measurement and modeling of orogenic fluxes. Am. J. Sci. 305, 369–406.
Spray, J.G., 2010. Frictional melting processes in planetary materials: from hypervelocity impact to earthquakes. Annu. Rev. Earth Planet Sci. 38, 221–254.
Spry, A., 1969. Metamorphic Textures. Pergamon Press Ltd., Oxford.
Swanson, M.T., 1988. Pseudotachylyte-bearing strike-slip duplex structures in the fort foster brittle zone, S. Maine. J. Struct. Geol. 10, 813–828.
Swanson, M.T., 1992. Fault structure, wear mechanisms and rupture processes in pseudotachylyte generation. Tectonophysics 204, 223–242.
Toy, V.G., Ritchie, S., Sibson, R.H., 2011. Diverse habitats of pseudotachylytes in the Alpine Fault Zone and relationships to current seismicity. Geol. Soc. London Spec. Publ. 359, 115–133. https://doi.org/10.1144/SP359.7.
van Hinsbergen, D.J.J., Torsvik, T.H., Schmid, S.M., Maţenco, L.C., Maffione, M., Vissers, R.L.M., Gürer, D., Spakman, W., 2019. Orogenic Architecture of the Mediterranean Region and Kinematic Reconstruction of its Tectonic Evolution since the Triassic: Gondwana Research, pp. 1–427. https://doi.org/10.1016/j.gr.2019.07.009.
Vergés, J., Millan, H., Roca, E., Muñoz, J.A., Marzo, M., Cirés, J., den Bezemer, T., Zoetemeijer, R., Cloethingh, S., 1995. Eastern Pyrenees and related foreland basins: pre-, syn- and post-collisional crustal-scale cross-sections. Mar. Petrol. Geol. 12, 903–916.
Vissers, R.L.M., Meijer, P.Th, 2012. Iberian plate kinematics and Alpine collision in the Pyrenees. Earth Sci. Rev. 114, 61–83. https://doi.org/10.1016/j.earscirev.2012.05.001.
Vissers, R., van Hinsbergen, D., Meijer, P.T., Piccardo, G.B., 2013. Kinematics of jurassic ultra-slow spreading in the piemonte ligurian ocean. Earth Planet Sci. Lett. 380, 138–150.
Vissers, R.L.M., van Hinsbergen, D.J.J., Wilkinson, C.M., Ganerød, M., 2017. Middle jurassic shear zones at Cap de Creus (E Pyrenees, Spain): a record of pre-drift extension of the piemonte-ligurian ocean? J. Geol. Soc. Lond. 174, 289–300.
Wenk, H.R., Weiss, L.E., 1982. Al-rich calcic pyroxene in pseudotachylyte: an indicator of high pressure and high temperature? Tectonophysics 84, 329–341.
Wenk, H.R., Johnson, L.R., Ratschbacher, L., 2000. Pseudotachylytes in the eastern peninsular ranges of California. Tectonophysics 321, 253–277.
Wyss, M., Brune, J.N., 1968. Seismic moment, stress, and source dimensions for earthquakes in the California–Nevada region. J. Geophys. Res. 73, 4681–4694.
Zanchetta, S., d'Adda, P., Zanchi, A., Barberini, V., Villa, I.M., 2011. Cretaceous-Eocene compression in the central Southern Alps (N Italy) inferred from ^{40}Ar-^{39}Ar dating of pseudotachylyites along regional thrust faults. J. Geodyn. 51, 245–263.
Zwart, H.J., 1979. The geology of the central Pyrenees. Leidse Geol. Meded. 50, 1–74.